International Journal of Mechanical Sciences 89 (2014) 242–255

Contents lists available at ScienceDirect

International Journal of Mechanical Sciences

journal homepage: www.elsevier.com/locate/ijmecsci

Geometrically-induced singularities in functionally graded magneto-electro-elastic wedges

C.S. Huang *, C.N. Hu

Department of Civil Engineering, National Chiao Tung University, 1001 Ta-Hsueh Road, Hsinchu 30050, Taiwan

ARTICLE INFO

Article history:
Received 13 November 2013
Received in revised form
10 April 2014
Accepted 14 September 2014
Available online 19 September 2014

Keywords:
Singularities
Magnet-electro-elastic wedge
Functional graded material
Three-dimensional asymptotic solution

ABSTRACT

Asymptotic solutions are proposed for geometrically-induced magneto-electro-elastic (MEE) singularities at the vertex of a rectilinearly polarized wedge that is made of functionally graded magneto-electro-elastic (FGMEE) materials. The material properties are assumed to vary along the thickness of the wedge, and the direction of polarization may not be parallel or perpendicular to the thickness direction. An eigenfunction expansion approach with the power series solution technique and domain decomposition is adopted to establish the asymptotic solutions by directly solving the three-dimensional equations of motion and Maxwell's equations in terms of mechanical displacement components and electric and magnetic potentials. Since the direction of polarization can be arbitrary in space, the in-plane components of displacement, electric and magnetic fields are generally coupled with the out-of-plane components. The solutions are presented here for the first time. The correctness of the proposed solutions is confirmed by comparing the orders of MEE singularities with the published results for wedges under anti-plane deformation and in-plane electric and magnetic fields. The proposed solutions are further employed to investigate the effects of the direction of polarization, vertex angle, boundary conditions and material-property gradient index on the MEE singularities in $BaTiO_3$–$CoFe_2O_4$ wedges.

1. Introduction

Magneto-electro-elastic (MEE) materials exhibit mechanical-electric-magnetic coupling effects and have a wide range of applications in engineering structures, while functionally graded materials (FGMs) have the special feature of graded spatial compositions, which affords freedom in the design and manufacturing of novel structures. It is interesting and important to investigate geometrically-induced magneto-electro-elastic singularities in wedges made of functionally graded magneto-electro-elastic (FGMEE) materials because such singularities normally initiate cracking and worsen the functioning of structures.

Numerous studies of geometrically-induced stress singularities in elastic wedges have been conducted, and most of them were reviewed by Sinclair [1]. Williams [2,3] was at the forefront of investigating stress singularities at the vertex of an elastic wedge under extension or bending. Following his work, various investigations have been carried out on elastic wedges that are made of single and multiple materials, drawing on plane elasticity theory [4–12], plate theories [13–16], and three-dimensional elasticity theory [17,18]. Huang and Chang [19,20] examined geometrically-induced stress singularities in FGM plates using classical plate theory and third-order shear deformation theory.

A few studies of geometrically-induced electroelastic singularities in piezoelectric wedges have been performed, and most of them make the plane strain assumption or the generalized plane deformation assumption. Using the plane strain assumption, Xu and Rajapakse [21] employed Lekhnitskii's complex potential functions to examine the in-plane electroelastic singularities at the vertex of a piezoelectric wedge, while Shang and Kitamura [22] utilized a modified version of the general solution of Wang and Zheng [23]. Hwu and Ikeda [24] made the generalized plane strain assumption and proposed an extended Stroh formulation to investigate the in-plane and out-of-plane electroelastic singularities in wedges. Chu et al. [25–27] adopted the generalized plane deformation assumption and conducted a series of analytical studies of geometrically-induced electroelastic singularities. Scherzer and Kuna [28], Chen et al. [29] and Chen and Ping [30] presented finite element solutions for in-plane singular electroelastic states at the vertex of a wedge. Based on the three-dimensional piezoelasticity theory, Huang and Hu [31] proposed asymptotic solutions at the vertex of a wedge.

Several studies have addressed magneto-electro-elastic singularities in MEE wedges and all of them considered wedges under

* Corresponding author.
E-mail address: cshuang@mail.nctu.edu.tw (C.S. Huang).

http://dx.doi.org/10.1016/j.ijmecsci.2014.09.009
0020-7403/

anti-plane deformation and in-plane electric and magnetic fields and assumed that all of the physical quantities are independent of the coordinates along the thickness. Liu and Chue [32] applied the Mellin transform to analyze the singularities at the vertex of a bi-material MEE wedge, while Sue et al. [33] employed the complex potential function with an eigenfunction expansion method. Liu [34] extended the solution of Liu and Chue [32] to examine the magneto-electro-elastic singularities at the apex of an MEE wedge-junction structure, accounting for the air effect.

A review of the literature reveals a complete lack of investigation of geometrically-induced magneto-electro-elastic singularities in MEE wedges and FGMEE wedges based on the three-dimensional magneto-electro-elasticity theory. Accordingly, this paper aims to derive a three-dimensional asymptotic solution for the MEE singularities at the vertex of an FGMEE wedge with an arbitrary direction of polarization by extending the solutions of Huang and Hu [31] for a piezoelectric wedge. The eigenfunction expansion method is combined with the power series technique and a domain decomposition scheme to solve the three-dimensional equations of motion and Maxwell's equations in terms of mechanical displacement components, electric potential and magnetic potential in a cylindrical coordinate system. The correctness of the proposed solution is confirmed by comparison with the published results of Liu and Chue [32] for MEE wedges under anti-plane deformation and in-plane electric and magnetic fields. The proposed solutions are further applied to determine the orders of the MEE singularities in $BaTiO_3$–$CoFe_2O_4$ wedges whose material properties may vary along the thickness. The results demonstrate the influence of the orientation of polarization, vertex angle, material-property gradient index and boundary conditions on the orders of MEE singularities in a wedge.

2. Basic equations of 3D magneto-electro-elasticity

Consider an FGMEE wedge with vertex angle β, shown in Fig. 1, where the $\bar{x}$–$\bar{y}$–$\bar{z}$ coordinate system is used to describe the material anisotropy, and the x–y–z coordinate system is used to describe the geometry of the wedge. The FGMEE material is assumed to be a transversely isotropic material with the polarization direction along the $\bar{z}$ axis. The material properties are assumed to vary along the z axis. The $\bar{x}$–$\bar{y}$–$\bar{z}$ coordinate system is not generally coincident with the x–y–z coordinate system, so the in-plane and out-of-plane physical quantities (mechanical displacement, electric and magnetic fields) are generally coupled.

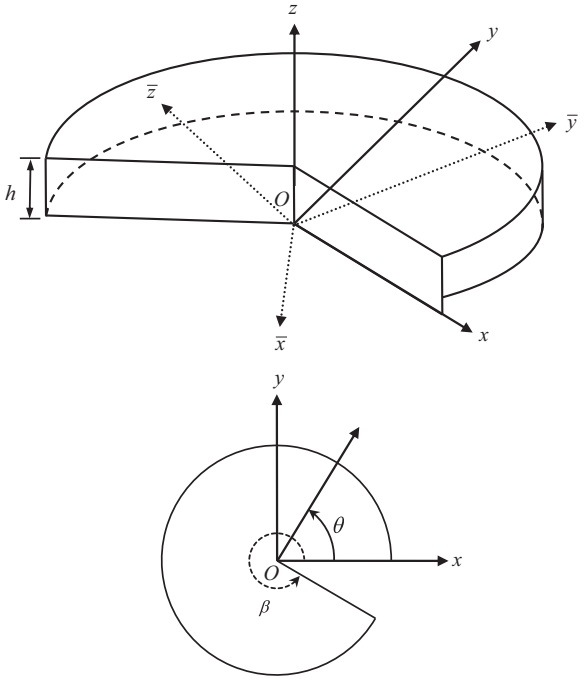

Fig. 1. Coordinate systems for a wedge.

The linear constitutive equations for the FGMEE material in the $\bar{x}$–$\bar{y}$–$\bar{z}$ coordinate are given by

$$\{\bar{\sigma}\} = [\bar{c}]\{\bar{\varepsilon}\} - [\bar{e}]^T\{\bar{E}\} - [\bar{d}]^T\{\bar{H}\}, \tag{1a}$$

$$\{\bar{D}\} = [\bar{e}]\{\bar{\varepsilon}\} + [\bar{\eta}]\{\bar{E}\} + [\bar{g}]\{\bar{H}\}, \tag{1b}$$

$$\{\bar{B}\} = [\bar{e}]\{\bar{\varepsilon}\} + [\bar{g}]\{\bar{E}\} + [\bar{\mu}]\{\bar{H}\}, \tag{1c}$$

where $\{\bar{\sigma}\} = \{\sigma_{\bar{x}\bar{x}} \;\; \sigma_{\bar{y}\bar{y}} \;\; \sigma_{\bar{z}\bar{z}} \;\; \sigma_{\bar{y}\bar{z}} \;\; \sigma_{\bar{z}\bar{x}} \;\; \sigma_{\bar{x}\bar{y}}\}^T$ and $\{\bar{\varepsilon}\} = \{\varepsilon_{\bar{x}\bar{x}} \;\; \varepsilon_{\bar{y}\bar{y}} \;\; \varepsilon_{\bar{z}\bar{z}} \;\; 2\varepsilon_{\bar{y}\bar{z}} \;\; 2\varepsilon_{\bar{z}\bar{x}} \;\; 2\varepsilon_{\bar{x}\bar{y}}\}^T$ are the stress and strain vectors, respectively; $\{\bar{D}\} = \{D_{\bar{x}} \;\; D_{\bar{y}} \;\; D_{\bar{z}}\}^T$ and $\{\bar{B}\} = \{B_{\bar{x}} \;\; B_{\bar{y}} \;\; B_{\bar{z}}\}^T$ are the electric displacement and magnetic flux vectors, respectively; $\{\bar{E}\} = \{E_{\bar{x}} \;\; E_{\bar{y}} \;\; E_{\bar{z}}\}^T$ and $\{\bar{H}\} = \{H_{\bar{x}} \;\; H_{\bar{y}} \;\; H_{\bar{z}}\}^T$ are the vectors of the electric and magnetic fields, respectively.

$$[\bar{c}] = \begin{bmatrix} \bar{c}_{11} & \bar{c}_{12} & \bar{c}_{13} & 0 & 0 & 0 \\ \bar{c}_{12} & \bar{c}_{11} & \bar{c}_{13} & 0 & 0 & 0 \\ \bar{c}_{13} & \bar{c}_{13} & \bar{c}_{33} & 0 & 0 & 0 \\ 0 & 0 & 0 & \bar{c}_{44} & 0 & 0 \\ 0 & 0 & 0 & 0 & \bar{c}_{44} & 0 \\ 0 & 0 & 0 & 0 & 0 & \frac{\bar{c}_{11}-\bar{c}_{12}}{2} \end{bmatrix},$$

$$[\bar{e}] = \begin{bmatrix} 0 & 0 & 0 & 0 & \bar{e}_{15} & 0 \\ 0 & 0 & 0 & \bar{e}_{15} & 0 & 0 \\ \bar{e}_{31} & \bar{e}_{31} & \bar{e}_{33} & 0 & 0 & 0 \end{bmatrix}$$

$$[\bar{d}] = \begin{bmatrix} 0 & 0 & 0 & 0 & \bar{d}_{15} & 0 \\ 0 & 0 & 0 & \bar{d}_{15} & 0 & 0 \\ \bar{d}_{31} & \bar{d}_{31} & \bar{d}_{33} & 0 & 0 & 0 \end{bmatrix},$$

$$[\bar{\eta}] = \begin{bmatrix} \bar{\eta}_{11} & 0 & 0 \\ 0 & \bar{\eta}_{11} & 0 \\ 0 & 0 & \bar{\eta}_{33} \end{bmatrix}, \quad [\bar{\mu}] = \begin{bmatrix} \bar{\mu}_{11} & 0 & 0 \\ 0 & \bar{\mu}_{11} & 0 \\ 0 & 0 & \bar{\mu}_{33} \end{bmatrix},$$

$$[\bar{g}] = \begin{bmatrix} \bar{g}_{11} & 0 & 0 \\ 0 & \bar{g}_{11} & 0 \\ 0 & 0 & \bar{g}_{33} \end{bmatrix}. \tag{2}$$

where $[\bar{c}]$, $[\bar{e}]$, $[\bar{d}]$, $[\bar{\eta}]$, $[\bar{\mu}]$ and $[\bar{g}]$ are the elastic stiffness constant, piezoelectric coefficient, piezomagnetic coefficient, dielectric constant, magnetic permeability, and magnetoelectric coefficient matrices, respectively, and all of these are functions of z.

The cylindrical coordinate system (r,θ,z) (Fig. 1) is used to investigate the MEE singularities as r approaches zero in the wedge. Hence, Eqs. (1) and (2) have to be transformed to (r,θ,z) from $(\bar{x},\bar{y},\bar{z})$ and rewritten as

$$\{\sigma\} = [c]\{\varepsilon\} - [e]^T\{E\} - [d]^T\{H\}, \tag{3a}$$

$$\{D\} = [e]\{\varepsilon\} + [\eta]\{E\} + [g]\{H\}, \tag{3b}$$

$$\{B\} = [d]\{\varepsilon\} + [g]\{E\} + [\mu]\{H\}, \tag{3c}$$

where

$$[c]=\begin{bmatrix} c_{11} & c_{12} & c_{13} & c_{14} & c_{15} & c_{16} \\ c_{12} & c_{22} & c_{23} & c_{24} & c_{25} & c_{26} \\ c_{13} & c_{23} & c_{33} & c_{34} & c_{35} & c_{36} \\ c_{14} & c_{24} & c_{34} & c_{44} & c_{45} & c_{46} \\ c_{15} & c_{25} & c_{35} & c_{45} & c_{55} & c_{56} \\ c_{16} & c_{26} & c_{36} & c_{46} & c_{56} & c_{66} \end{bmatrix},$$

$$[e]=\begin{bmatrix} e_{11} & e_{12} & e_{13} & e_{14} & e_{15} & e_{16} \\ e_{21} & e_{22} & e_{23} & e_{24} & e_{25} & e_{26} \\ e_{31} & e_{32} & e_{33} & e_{34} & e_{35} & e_{36} \end{bmatrix}$$

$$[d]=\begin{bmatrix} d_{11} & d_{12} & d_{13} & d_{14} & d_{15} & d_{16} \\ d_{21} & d_{22} & d_{23} & d_{24} & d_{25} & d_{26} \\ d_{31} & d_{32} & d_{33} & d_{34} & d_{35} & d_{36} \end{bmatrix},$$

$$[\eta]=\begin{bmatrix} \eta_{11} & \eta_{12} & \eta_{13} \\ \eta_{12} & \eta_{22} & \eta_{23} \\ \eta_{13} & \eta_{23} & \eta_{33} \end{bmatrix}, \quad [\mu]=\begin{bmatrix} \mu_{11} & \mu_{12} & \mu_{13} \\ \mu_{12} & \mu_{22} & \mu_{23} \\ \mu_{13} & \mu_{23} & \mu_{33} \end{bmatrix},$$

$$[g]=\begin{bmatrix} g_{11} & g_{12} & g_{13} \\ g_{12} & g_{22} & g_{23} \\ g_{13} & g_{23} & g_{33} \end{bmatrix}.$$

Now the material properties matrices $[c]$, $[e]$, $[d]$, $[\eta]$, $[\mu]$ and $[g]$ are related to $[\bar{c}]$, $[\bar{e}]$, $[\bar{d}]$, $[\bar{\eta}]$, $[\bar{\mu}]$ and $[\bar{g}]$, respectively, and are the functions of θ, z and the angles between the axes of $\bar{x}$–$\bar{y}$–$\bar{z}$ and x–y–z. These relations are specified in Appendix A.

To develop the asymptotic solutions to examine the geometrically-induced magneto-electro-elastic singularities as r approaches zero in a wedge, the body forces, free electric charges and magnetic charges are ignored, and the equations of motion and Maxwell's equations are

$$\frac{\partial\sigma_{rr}}{\partial r}+\frac{1}{r}\frac{\partial\sigma_{r\theta}}{\partial\theta}+\frac{\partial\sigma_{rz}}{\partial z}+\frac{(\sigma_{rr}-\sigma_{\theta\theta})}{r}=\rho^*\frac{\partial^2 u_r^*}{\partial t^2}, \tag{4a}$$

$$\frac{\partial\sigma_{r\theta}}{\partial r}+\frac{1}{r}\frac{\partial\sigma_{\theta\theta}}{\partial\theta}+\frac{\partial\sigma_{\theta z}}{\partial z}+2\frac{\sigma_{r\theta}}{r}=\rho^*\frac{\partial^2 u_\theta^*}{\partial t^2}, \tag{4b}$$

$$\frac{\partial\sigma_{rz}}{\partial r}+\frac{1}{r}\frac{\partial\sigma_{\theta z}}{\partial\theta}+\frac{\partial\sigma_{zz}}{\partial z}+\frac{\sigma_{rz}}{r}=\rho^*\frac{\partial^2 u_z^*}{\partial t^2}, \tag{4c}$$

$$\frac{1}{r}\frac{\partial(rD_r)}{\partial r}+\frac{1}{r}\frac{\partial D_\theta}{\partial\theta}+\frac{\partial D_z}{\partial z}=0, \tag{4d}$$

$$\frac{1}{r}\frac{\partial(rB_r)}{\partial r}+\frac{1}{r}\frac{\partial B_\theta}{\partial\theta}+\frac{\partial B_z}{\partial z}=0, \tag{4e}$$

where ρ^* is the density of the material, and u_i^* $(i=r,\theta,z)$ is the displacement component in the i direction.

Using electric field-electric potential and magnetic field-magnetic potential relations,

$$E_r=-\frac{\partial\phi^*}{\partial r},\ E_\theta=-\frac{1}{r}\frac{\partial\phi^*}{\partial\theta},\ E_z=-\frac{\partial\phi^*}{\partial z},$$
$$H_r=-\frac{\partial\psi^*}{\partial r},\ H_\theta=-\frac{1}{r}\frac{\partial\psi^*}{\partial\theta}\ \text{and}\ H_z=-\frac{\partial\psi^*}{\partial z}, \tag{5}$$

as well as the strain–displacement relations, Eqs. (4a)–(4e) can be expressed in terms of mechanical displacement components (u_r^*, u_θ^* and u_z^*), electric potential (ϕ^*) and magnetic potential (ψ^*) as follows:

$$\begin{aligned}&\left[c_{11}\frac{\partial^2}{\partial r^2}+\left(\frac{c_{66}}{r^2}\right)\frac{\partial^2}{\partial\theta^2}+c_{55}\frac{\partial^2}{\partial z^2}+\left(\frac{2c_{16}}{r}\right)\frac{\partial^2}{\partial r\,\partial\theta}\right.\\&\quad+2c_{15}\frac{\partial^2}{\partial r\,\partial z}+\left(\frac{2c_{56}}{r}\right)\frac{\partial^2}{\partial\theta\,\partial z}+\left(c_{11}+\frac{\partial c_{16}}{\partial\theta}+r\frac{\partial c_{15}}{\partial z}\right)\frac{\partial}{r\partial r}\\&\quad+\left(\frac{\partial c_{66}}{\partial\theta}+r\frac{\partial c_{56}}{\partial z}\right)\frac{\partial}{r^2\partial\theta}+\left(c_{15}+\frac{\partial c_{56}}{\partial\theta}+r\frac{\partial c_{55}}{\partial z}\right)\frac{\partial}{r\partial z}\\&\quad+\left(-c_{22}+\frac{\partial c_{26}}{\partial\theta}+r\frac{\partial c_{25}}{\partial z}\right)\frac{1}{r^2}-\rho^*\frac{\partial^2}{\partial t^2}\Big]u_r^*\\&\quad+\left[c_{16}\frac{\partial^2}{\partial r^2}+\left(\frac{c_{26}}{r^2}\right)\frac{\partial^2}{\partial\theta^2}+c_{45}\frac{\partial^2}{\partial z^2}+(c_{12}+c_{66})\frac{\partial^2}{r\partial r\,\partial\theta}\right.\\&\quad+(c_{14}+c_{56})\frac{\partial^2}{\partial r\,\partial z}+(c_{25}+c_{46})\frac{\partial^2}{r\partial\theta\,\partial z}\\&\quad+\left(-c_{26}+\frac{\partial c_{66}}{\partial\theta}+r\frac{\partial c_{56}}{\partial z}\right)\frac{\partial}{r\partial r}\\&\quad+\left(-c_{22}-c_{66}+\frac{\partial c_{26}}{\partial\theta}+r\frac{\partial c_{25}}{\partial z}\right)\frac{\partial}{r^2\partial\theta}\\&\quad+\left(c_{14}-c_{24}-c_{56}+\frac{\partial c_{46}}{\partial\theta}+r\frac{\partial c_{45}}{\partial z}\right)\\&\quad\times\frac{\partial}{r\partial z}+\left(c_{26}-\frac{\partial c_{66}}{\partial\theta}-\frac{\partial c_{56}}{\partial z}\right)\frac{1}{r^2}\Big]u_\theta^*\\&\quad+\left[c_{15}\frac{\partial^2}{\partial r^2}+\left(\frac{c_{46}}{r^2}\right)\frac{\partial^2}{\partial\theta^2}+c_{35}\frac{\partial^2}{\partial z^2}+(c_{14}+c_{56})\frac{\partial^2}{r\partial r\,\partial\theta}+(c_{13}+c_{55})\right.\\&\quad\times\frac{\partial^2}{\partial r\,\partial z}+(c_{36}+c_{45})\frac{\partial^2}{r\partial\theta\,\partial z}+\left(c_{15}-c_{25}+\frac{\partial c_{56}}{\partial\theta}+r\frac{\partial c_{55}}{\partial z}\right)\frac{\partial}{r\partial r}\\&\quad+\left(-c_{24}+\frac{\partial c_{46}}{\partial\theta}+r\frac{\partial c_{45}}{\partial z}\right)\frac{\partial}{r^2\partial\theta}\\&\quad+\left(c_{13}-c_{23}+\frac{\partial c_{36}}{\partial\theta}+r\frac{\partial c_{35}}{\partial z}\right)\frac{\partial}{r\partial z}\Big]u_z^*\\&\quad+\left[e_{11}\frac{\partial^2}{\partial r^2}+\left(\frac{e_{26}}{r^2}\right)\frac{\partial^2}{\partial\theta^2}+e_{35}\frac{\partial^2}{\partial z^2}+(e_{16}+e_{21})\frac{\partial^2}{r\partial r\,\partial\theta}\right.\\&\quad+(e_{15}+e_{31})\frac{\partial^2}{\partial r\,\partial z}+(e_{25}+e_{36})\frac{\partial^2}{r\partial\theta\,\partial z}\\&\quad+\left(e_{11}-e_{12}+\frac{\partial e_{16}}{\partial\theta}+r\frac{\partial e_{15}}{\partial z}\right)\frac{\partial}{r\partial r}+\left(-e_{22}+\frac{\partial e_{26}}{\partial\theta}+r\frac{\partial e_{25}}{\partial z}\right)\frac{\partial}{r^2\partial\theta}\\&\quad+\left(e_{31}-e_{32}+\frac{\partial e_{36}}{\partial\theta}+r\frac{\partial e_{35}}{\partial z}\right)\frac{\partial}{r\partial z}\Big]\phi^*\\&\quad+\left[d_{11}\frac{\partial^2}{\partial r^2}+\left(\frac{d_{26}}{r^2}\right)\frac{\partial^2}{\partial\theta^2}+d_{35}\frac{\partial^2}{\partial z^2}+(d_{16}+d_{21})\frac{\partial^2}{r\partial r\,\partial\theta}\right.\\&\quad+(d_{15}+d_{31})\frac{\partial^2}{\partial r\,\partial z}+(d_{25}+d_{36})\frac{\partial^2}{r\partial\theta\,\partial z}\\&\quad+\left(d_{11}-d_{12}+\frac{\partial d_{16}}{\partial\theta}+r\frac{\partial d_{15}}{\partial z}\right)\frac{\partial}{r\partial r}+\left(-d_{22}+\frac{\partial d_{26}}{\partial\theta}+r\frac{\partial d_{16}}{\partial z}\right)\\&\quad\times\frac{\partial}{r^2\partial\theta}+\left(d_{31}-d_{32}+\frac{\partial d_{36}}{\partial\theta}+r\frac{\partial d_{36}}{\partial z}\right)\frac{\partial}{r\partial z}\Big]\psi^*=0,\end{aligned} \tag{6a}$$

$$\begin{aligned}&\left[c_{16}\frac{\partial^2}{\partial r^2}+\left(\frac{c_{26}}{r^2}\right)\frac{\partial^2}{\partial\theta^2}+c_{45}\frac{\partial^2}{\partial z^2}+(c_{12}+c_{66})\frac{\partial^2}{r\partial r\,\partial\theta}\right.\\&\quad+(c_{14}+c_{56})\frac{\partial^2}{\partial r\,\partial z}+(c_{25}+c_{46})\frac{\partial^2}{r\partial\theta\,\partial z}+\left(2c_{16}+c_{26}+\frac{\partial c_{12}}{\partial\theta}+r\frac{\partial c_{14}}{\partial z}\right)\frac{\partial}{r\partial r}\\&\quad+\left(c_{22}+c_{66}+\frac{\partial c_{26}}{\partial\theta}+r\frac{\partial c_{46}}{\partial z}\right)\frac{\partial}{r^2\partial\theta}+\left(c_{24}+2c_{56}+\frac{\partial c_{25}}{\partial\theta}+r\frac{\partial c_{45}}{\partial z}\right)\\&\quad\times\frac{\partial}{r\partial z}+\left(c_{26}+\frac{\partial c_{22}}{\partial\theta}+r\frac{\partial c_{24}}{\partial z}\right)\frac{1}{r^2}\Big]u_r^*+\left[c_{66}\frac{\partial^2}{\partial r^2}+\left(\frac{c_{22}}{r^2}\right)\frac{\partial^2}{\partial\theta^2}+c_{44}\frac{\partial^2}{\partial z^2}\right.\\&\quad+\left(\frac{2c_{26}}{r}\right)\frac{\partial^2}{\partial r\,\partial\theta}+2c_{46}\frac{\partial^2}{\partial r\,\partial z}+2c_{24}\frac{\partial^2}{r\partial\theta\,\partial z}\\&\quad+\left(c_{66}+\frac{\partial c_{26}}{\partial\theta}+r\frac{\partial c_{46}}{\partial z}\right)\frac{\partial}{r\partial r}+\left(\frac{\partial c_{22}}{\partial\theta}+r\frac{\partial c_{24}}{\partial z}\right)\frac{\partial}{r^2\partial\theta}\\&\quad+\left(c_{46}+\frac{\partial c_{24}}{\partial\theta}+r\frac{\partial c_{44}}{\partial z}\right)\frac{\partial}{r\partial z}+\left(-c_{66}-\frac{\partial c_{26}}{\partial\theta}-r\frac{\partial c_{46}}{\partial z}\right)\frac{1}{r^2}-\rho^*\frac{\partial^2}{\partial t^2}\Big]u_\theta^*\\&\quad+\left[c_{56}\frac{\partial^2}{\partial r^2}+\left(\frac{c_{24}}{r^2}\right)\frac{\partial^2}{\partial\theta^2}+c_{34}\frac{\partial^2}{\partial z^2}+(c_{25}+c_{46})\frac{\partial^2}{r\partial r\,\partial\theta}\right.\\&\quad+(c_{36}+c_{45})\frac{\partial^2}{\partial r\,\partial z}+(c_{23}+c_{44})\frac{\partial^2}{r\partial\theta\,\partial z}+\left(2c_{56}+\frac{\partial c_{25}}{\partial\theta}+r\frac{\partial c_{45}}{\partial z}\right)\frac{\partial}{r\partial r}\\&\quad+\left(c_{46}+\frac{\partial c_{24}}{\partial\theta}+r\frac{\partial c_{44}}{\partial z}\right)\frac{\partial}{r^2\partial\theta}+\left(2c_{36}+\frac{\partial c_{23}}{\partial\theta}+r\frac{\partial c_{34}}{\partial z}\right)\frac{\partial}{r\partial z}\Big]u_z^*\end{aligned}$$

$$+\left[e_{16}\frac{\partial^2}{\partial r^2}+\left(\frac{e_{22}}{r^2}\right)\frac{\partial^2}{\partial\theta^2}+e_{34}\frac{\partial^2}{\partial z^2}+(e_{12}+e_{26})\frac{\partial^2}{r\partial r\,\partial\theta}+(e_{14}+e_{36})\right.$$
$$\times\frac{\partial^2}{\partial r\,\partial z}+(e_{24}+e_{32})\frac{\partial^2}{r\partial\theta\,\partial z}+\left(2e_{16}+\frac{\partial e_{12}}{\partial\theta}+r\frac{\partial e_{14}}{\partial z}\right)\frac{\partial}{r\partial r}$$
$$+\left(e_{26}+\frac{\partial e_{22}}{\partial\theta}+r\frac{\partial e_{24}}{\partial z}\right)\frac{\partial}{r^2\partial\theta}+\left(2e_{36}+\frac{\partial e_{32}}{\partial\theta}\right.$$
$$\left.+r\frac{\partial e_{34}}{\partial z}\right)\frac{\partial}{r\partial z}\Big]\phi^*+\left[d_{16}\frac{\partial^2}{\partial r^2}+\left(\frac{d_{22}}{r^2}\right)\frac{\partial^2}{\partial\theta^2}+d_{34}\frac{\partial^2}{\partial z^2}+(d_{12}+d_{26})\frac{\partial^2}{r\partial r\,\partial\theta}\right.$$
$$+(d_{14}+d_{36})\frac{\partial^2}{\partial r\,\partial z}+(d_{24}+d_{32})\frac{\partial^2}{r\partial\theta\,\partial z}+\left(2d_{16}+\frac{\partial d_{12}}{\partial\theta}+r\frac{\partial d_{14}}{\partial z}\right)\frac{\partial}{r\partial r}$$
$$\left.+\left(d_{26}+\frac{\partial d_{22}}{\partial\theta}+r\frac{\partial d_{24}}{\partial z}\right)\frac{\partial}{r^2\partial\theta}+\left(2d_{36}+\frac{\partial d_{32}}{\partial\theta}+r\frac{\partial d_{34}}{\partial z}\right)\frac{\partial}{r\partial z}\right]\psi^*=0, \tag{6b}$$

$$\left[c_{15}\frac{\partial^2}{\partial r^2}+\left(\frac{c_{46}}{r^2}\right)\frac{\partial^2}{\partial\theta^2}+c_{35}\frac{\partial^2}{\partial z^2}+(c_{14}+c_{56})\frac{\partial^2}{r\partial r\,\partial\theta}+(c_{13}+c_{55})\frac{\partial^2}{\partial r\,\partial z}\right.$$
$$+(c_{36}+c_{45})\frac{\partial^2}{r\partial\theta\,\partial z}+\left(c_{15}+c_{25}+\frac{\partial c_{14}}{\partial\theta}+r\frac{\partial c_{13}}{\partial z}\right)\frac{\partial}{r\partial r}$$
$$+\left(c_{24}+\frac{\partial c_{46}}{\partial\theta}+r\frac{\partial c_{36}}{\partial z}\right)\frac{\partial}{r^2\partial\theta}+\left(c_{23}+c_{55}+\frac{\partial c_{45}}{\partial\theta}+r\frac{\partial c_{35}}{\partial z}\right)\frac{\partial}{r\partial z}$$
$$+\left(\frac{\partial c_{24}}{\partial\theta}+r\frac{\partial c_{23}}{\partial z}\right)\frac{1}{r^2}\Big]u_r^*+\left[c_{56}\frac{\partial^2}{\partial r^2}+\left(\frac{c_{24}}{r^2}\right)\frac{\partial^2}{\partial\theta^2}\right.$$
$$+c_{34}\frac{\partial^2}{\partial z^2}+(c_{25}+c_{46})\frac{\partial^2}{r\partial r\,\partial\theta}+(c_{36}+c_{45})\frac{\partial^2}{\partial r\,\partial z}$$
$$+(c_{23}+c_{44})\frac{\partial^2}{r\partial\theta\,\partial z}+\left(\frac{\partial c_{46}}{\partial\theta}+r\frac{\partial c_{36}}{\partial z}\right)\frac{\partial}{r\partial r}$$
$$+\left(-c_{46}+\frac{\partial c_{24}}{\partial\theta}+r\frac{\partial c_{23}}{\partial z}\right)\frac{\partial}{r^2\partial\theta}+\left(-c_{36}+c_{45}+\frac{\partial c_{44}}{\partial\theta}\right.$$
$$\left.+r\frac{\partial c_{34}}{\partial\theta}\right)\frac{\partial}{r\partial z}+\left(-\frac{\partial c_{46}}{\partial\theta}-r\frac{\partial c_{36}}{\partial z}\right)\frac{1}{r^2}\Big]u_\theta^*$$
$$+\left[c_{55}\frac{\partial^2}{\partial r^2}+\left(\frac{c_{44}}{r^2}\right)\frac{\partial^2}{\partial\theta^2}+c_{33}\frac{\partial^2}{\partial z^2}+\left(\frac{2c_{45}}{r}\right)\frac{\partial^2}{\partial r\,\partial\theta}+2c_{35}\right.$$
$$\times\frac{\partial}{r\partial z}-\rho^*\frac{\partial^2}{\partial t^2}\Big]u_z^*+\left[e_{15}\frac{\partial^2}{\partial r^2}+\left(\frac{e_{24}}{r^2}\right)\frac{\partial^2}{\partial\theta^2}\right.$$
$$+e_{33}\frac{\partial^2}{\partial z^2}+(e_{14}+e_{25})\frac{\partial^2}{r\partial r\,\partial\theta}+(e_{13}+e_{35})\frac{\partial^2}{\partial r\,\partial z}+(e_{23}$$
$$\times\frac{\partial^2}{\partial r\,\partial z}+\left(\frac{2c_{34}}{r}\right)\frac{\partial^2}{\partial\theta\,\partial z}+\left(c_{55}+\frac{\partial c_{45}}{\partial\theta}+r\frac{\partial c_{35}}{\partial z}\right)\frac{\partial}{r\partial r}$$
$$+\left(\frac{\partial c_{44}}{\partial\theta}+r\frac{\partial c_{34}}{\partial z}\right)\frac{\partial}{r^2\partial\theta}+\left(c_{35}+\frac{\partial c_{34}}{\partial\theta}+r\frac{\partial c_{33}}{\partial z}\right)$$
$$+e_{34})\frac{\partial^2}{r\partial\theta\,\partial z}+\left(e_{15}+\frac{\partial e_{14}}{\partial\theta}+r\frac{\partial e_{13}}{\partial z}\right)\frac{\partial}{r\partial r}$$
$$+\left(\frac{\partial e_{24}}{\partial\theta}+r\frac{\partial e_{23}}{\partial z}\right)\frac{\partial}{r^2\partial\theta}+\left(e_{35}+\frac{\partial e_{34}}{\partial\theta}+r\frac{\partial e_{33}}{\partial z}\right)\frac{\partial}{r\partial z}\Big]\phi^*$$
$$+\left[d_{15}\frac{\partial^2}{\partial r^2}+\left(\frac{d_{24}}{r^2}\right)\frac{\partial^2}{\partial\theta^2}+d_{33}\frac{\partial^2}{\partial z^2}+(d_{14}+d_{25})\frac{\partial^2}{r\partial r\,\partial\theta}\right.$$
$$+(d_{13}+d_{35})\frac{\partial^2}{\partial r\,\partial z}+(d_{23}+d_{34})\frac{\partial^2}{r\partial\theta\,\partial z}$$
$$+\left(d_{15}+\frac{\partial d_{14}}{\partial\theta}+r\frac{\partial d_{13}}{\partial z}\right)\frac{\partial}{r\partial r}+\left(\frac{\partial d_{24}}{\partial\theta}+r\frac{\partial d_{23}}{\partial z}\right)\frac{\partial}{r^2\partial\theta}$$
$$\left.+\left(d_{35}+\frac{\partial d_{34}}{\partial\theta}+r\frac{\partial d_{33}}{\partial z}\right)\frac{\partial}{r\partial z}\right]\psi^*=0, \tag{6c}$$

$$\left[e_{11}\frac{\partial^2}{\partial r^2}+\left(\frac{e_{26}}{r^2}\right)\frac{\partial^2}{\partial\theta^2}+e_{35}\frac{\partial^2}{\partial z^2}+(e_{16}+e_{21})\frac{\partial^2}{r\partial r\,\partial\theta}+(e_{15}+e_{31})\frac{\partial^2}{\partial r\,\partial z}\right.$$
$$+(e_{25}+e_{36})\frac{\partial^2}{r\partial\theta\,\partial z}+\left(e_{11}+e_{12}+\frac{\partial e_{21}}{\partial\theta}+r\frac{\partial e_{31}}{\partial z}\right)\frac{\partial}{r\partial r}$$
$$+\left(e_{22}+\frac{\partial e_{26}}{\partial\theta}+r\frac{\partial e_{36}}{\partial z}\right)\frac{\partial}{r^2\partial\theta}+\left(e_{15}+e_{32}+\frac{\partial e_{25}}{\partial\theta}+r\frac{\partial e_{35}}{\partial z}\right)\frac{\partial}{r\partial z}$$
$$+\left(\frac{\partial e_{22}}{\partial\theta}+r\frac{\partial e_{32}}{\partial z}\right)\times\frac{1}{r^2}\Big]u_r^*+\left[e_{16}\frac{\partial^2}{\partial r^2}+\left(\frac{e_{22}}{r^2}\right)\frac{\partial^2}{\partial\theta^2}\right.$$
$$+e_{34}\frac{\partial^2}{\partial z^2}+(e_{12}+e_{26})\frac{\partial^2}{r\partial r\,\partial\theta}+(e_{14}+e_{36})\frac{\partial^2}{r\partial r\,\partial z}+(e_{24}+e_{32})\frac{\partial^2}{r\partial\theta\,\partial z}$$
$$+\left(\frac{\partial e_{26}}{\partial\theta}+r\frac{\partial e_{36}}{\partial z}\right)\frac{\partial}{r\partial r}+\left(-e_{26}+\frac{\partial e_{22}}{\partial\theta}+r\frac{\partial e_{32}}{\partial z}\right)\frac{\partial}{r^2\partial\theta}$$
$$+\left(e_{14}-e_{36}+\frac{\partial e_{24}}{\partial\theta}+r\frac{\partial e_{34}}{\partial z}\right)\frac{\partial}{r\partial z}+\left(-\frac{\partial e_{26}}{\partial\theta}-r\frac{\partial e_{36}}{\partial z}\right)\frac{1}{r^2}\Big]u_\theta^*$$
$$+\left[e_{15}\frac{\partial^2}{\partial r^2}+\left(\frac{e_{24}}{r^2}\right)\frac{\partial^2}{\partial\theta^2}+e_{33}\frac{\partial^2}{\partial z^2}+(e_{14}+e_{25})\frac{\partial^2}{r\partial r\,\partial\theta}\right.$$
$$+(e_{13}+e_{35})\frac{\partial^2}{\partial r\,\partial z}+(e_{13}+e_{35})$$
$$\times\frac{\partial^2}{\partial r\,\partial z}+(e_{23}+e_{34})\frac{\partial^2}{r\partial\theta\,\partial z}+\left(e_{15}+\frac{\partial e_{25}}{\partial\theta}+r\frac{\partial e_{35}}{\partial z}\right)\frac{\partial}{r\partial r}$$
$$+\left(\frac{\partial e_{24}}{\partial\theta}+r\frac{\partial e_{25}}{\partial z}\right)\frac{\partial}{r^2\partial\theta}+\left(e_{13}+\frac{\partial e_{23}}{\partial\theta}+r\frac{\partial e_{33}}{\partial z}\right)\frac{\partial}{r\partial z}\Big]u_z^*$$
$$-\left[\eta_{11}\frac{\partial^2}{\partial r^2}+\left(\frac{\eta_{22}}{r^2}\right)\frac{\partial^2}{\partial\theta^2}+\eta_{33}\frac{\partial^2}{\partial z^2}+\left(\frac{2\eta_{12}}{r}\right)\frac{\partial^2}{\partial r\,\partial\theta}+2\eta_{13}\frac{\partial^2}{\partial r\,\partial z}\right.$$
$$+\left(\frac{2\eta_{23}}{r}\right)\frac{\partial^2}{\partial\theta\,\partial z}+\left(\eta_{11}+\frac{\partial\eta_{12}}{\partial\theta}+r\frac{\partial\eta_{13}}{\partial z}\right)\frac{\partial}{r\partial r}$$
$$+\left(\frac{\partial\eta_{22}}{\partial\theta}+r\frac{\partial\eta_{23}}{\partial z}\right)\frac{\partial}{r^2\partial\theta}+\left(\eta_{13}+\frac{\partial\eta_{23}}{\partial\theta}+r\frac{\partial\eta_{33}}{\partial z}\right)\frac{\partial}{r\partial z}\Big]\phi^*$$
$$-\left[g_{11}\frac{\partial^2}{\partial r^2}+\left(\frac{g_{22}}{r^2}\right)\frac{\partial^2}{\partial\theta^2}+g_{33}\frac{\partial^2}{\partial z^2}+\left(\frac{2g_{12}}{r}\right)\frac{\partial^2}{\partial r\,\partial\theta}\right.$$
$$+2g_{13}\frac{\partial^2}{\partial r\,\partial z}+\left(\frac{2g_{23}}{r}\right)\frac{\partial^2}{\partial\theta\,\partial z}+\left(g_{11}+\frac{\partial g_{12}}{\partial\theta}+r\frac{\partial g_{13}}{\partial z}\right)\frac{\partial}{r\partial r}$$
$$\left.+\left(\frac{\partial g_{22}}{\partial\theta}+r\frac{\partial g_{23}}{\partial z}\right)\frac{\partial}{r^2\partial\theta}+\left(g_{13}+\frac{\partial g_{23}}{\partial\theta}+r\frac{\partial g_{33}}{\partial z}\right)\frac{\partial}{r\partial z}\right]\psi^*=0, \tag{6d}$$

$$\left[d_{11}\frac{\partial^2}{\partial r^2}+\left(\frac{d_{26}}{r^2}\right)\frac{\partial^2}{\partial\theta^2}+d_{35}\frac{\partial^2}{\partial z^2}+(d_{16}+d_{21})\frac{\partial^2}{r\partial r\,\partial\theta}+(d_{15}+d_{31})\frac{\partial^2}{\partial r\,\partial z}\right.$$
$$+(d_{25}+d_{36})\frac{\partial^2}{r\partial\theta\,\partial z}+\left(d_{11}+d_{12}+\frac{\partial d_{21}}{\partial\theta}+r\frac{\partial d_{31}}{\partial z}\right)\frac{\partial}{r\partial r}$$
$$+\left(d_{22}+\frac{\partial d_{26}}{\partial\theta}+r\frac{\partial d_{36}}{\partial z}\right)\frac{\partial}{r^2\partial\theta}+\left(d_{15}+d_{32}+\frac{\partial d_{25}}{\partial\theta}+r\frac{\partial d_{35}}{\partial z}\right)\frac{\partial}{r\partial z}$$
$$+\left(\frac{\partial d_{22}}{\partial\theta}+r\frac{\partial d_{32}}{\partial z}\right)\frac{1}{r^2}\Big]u_r^*+\left[d_{16}\frac{\partial^2}{\partial r^2}+\left(\frac{d_{22}}{r^2}\right)\frac{\partial^2}{\partial\theta^2}+d_{34}\frac{\partial^2}{\partial z^2}\right.$$
$$+(d_{12}+d_{26})\frac{\partial^2}{r\partial r\,\partial\theta}+(d_{14}+d_{36})\frac{\partial^2}{\partial r\,\partial z}$$
$$+(d_{24}+d_{32})\frac{\partial^2}{r\partial\theta\,\partial z}+\left(\frac{\partial d_{26}}{\partial\theta}+r\frac{\partial d_{36}}{\partial z}\right)\frac{\partial}{r\partial r}$$
$$+\left(-d_{26}+\frac{\partial d_{22}}{\partial\theta}+r\frac{\partial d_{32}}{\partial z}\right)\frac{\partial}{r^2\partial\theta}+\left(d_{14}-d_{36}+\frac{\partial d_{24}}{\partial\theta}+r\frac{\partial d_{34}}{\partial z}\right)\frac{\partial}{r\partial z}$$
$$+\left(-\frac{\partial d_{26}}{\partial\theta}-r\frac{\partial d_{36}}{\partial z}\right)\frac{1}{r^2}\Big]u_\theta^*+\left[d_{15}\frac{\partial^2}{\partial r^2}+\left(\frac{d_{24}}{r^2}\right)\frac{\partial^2}{\partial\theta^2}+d_{33}\frac{\partial^2}{\partial z^2}\right.$$
$$+\left(d_{14}+d_{25}\right)\frac{\partial^2}{r\partial r\,\partial\theta}+(d_{13}+d_{35})\frac{\partial^2}{\partial r\,\partial z}+(d_{23}+d_{34})\frac{\partial^2}{r\partial\theta\,\partial z}$$
$$+\left(d_{15}+\frac{\partial d_{25}}{\partial\theta}+r\frac{\partial d_{35}}{\partial z}\right)\frac{\partial}{r\partial r}+\left(\frac{\partial d_{24}}{\partial\theta}+r\frac{\partial d_{34}}{\partial z}\right)\frac{\partial}{r^2\partial\theta}$$
$$+\left(d_{13}+\frac{\partial d_{23}}{\partial\theta}+r\frac{\partial d_{33}}{\partial z}\right)\frac{\partial}{r\partial z}\Big]u_z^*-\left[g_{11}\frac{\partial^2}{\partial r^2}+\left(\frac{g_{22}}{r^2}\right)\frac{\partial^2}{\partial\theta^2}+g_{33}\frac{\partial^2}{\partial z^2}\right.$$
$$+\left(\frac{2g_{12}}{r}\right)\frac{\partial^2}{\partial r\,\partial\theta}+2g_{13}\frac{\partial^2}{\partial r\,\partial z}+\left(\frac{2g_{23}}{r}\right)\times\frac{\partial^2}{\partial\theta\,\partial z}$$
$$+\left(g_{11}+\frac{\partial g_{12}}{\partial\theta}+r\frac{\partial g_{13}}{\partial z}\right)\frac{\partial}{r\partial r}+\left(\frac{\partial g_{22}}{\partial\theta}+r\frac{\partial g_{23}}{\partial z}\right)\frac{\partial}{r^2\partial\theta}$$
$$+\left(g_{13}+\frac{\partial g_{23}}{\partial\theta}+r\frac{\partial g_{33}}{\partial z}\right)\frac{\partial}{r\partial z}\Big]\phi^*$$
$$-\left[\mu_{11}\frac{\partial^2}{\partial r^2}+\left(\frac{\mu_{22}}{r^2}\right)\frac{\partial^2}{\partial\theta^2}+\mu_{33}\frac{\partial^2}{\partial z^2}+\left(\frac{2\mu_{12}}{r}\right)\frac{\partial^2}{\partial r\,\partial\theta}+2\mu_{13}\frac{\partial^2}{\partial r\,\partial z}\right.$$
$$+\left(\frac{2\mu_{23}}{r}\right)\frac{\partial^2}{\partial\theta\,\partial z}+\left(\mu_{11}+\frac{\partial\mu_{12}}{\partial\theta}+r\frac{\partial\mu_{13}}{\partial z}\right)\frac{\partial}{r\partial r}+\left(\frac{\partial\mu_{22}}{\partial\theta}+r\frac{\partial\mu_{23}}{\partial z}\right)\frac{\partial}{r^2\partial\theta}$$
$$\left.+\left(\mu_{13}+\frac{\partial\mu_{23}}{\partial\theta}+r\frac{\partial\mu_{33}}{\partial z}\right)\frac{\partial}{r\partial z}\right]\psi^*=0, \tag{6e}$$

3. Construction of asymptotic solution

The eigenfunction expansion approach, which Hartranft and Sih [7] had used for 3D elastic wedges, is adopted herein. The mechanical displacements, electric potential and magnetic potential are expressed as

$$u_r^*(r,\theta,z,t)=\left[\sum_{m=1}^{\infty}\sum_{n=0}^{\infty} r^{\lambda_m+n}\hat{U}_n^{(m)}(\theta,z)\right]e^{i\omega t}, \tag{7a}$$

$$u_\theta^*(r,\theta,z,t)=\left[\sum_{m=1}^{\infty}\sum_{n=0}^{\infty} r^{\lambda_m+n}\hat{V}_n^{(m)}(\theta,z)\right]e^{i\omega t}, \tag{7b}$$

$$u_z^*(r,\theta,z,t)=\left[\sum_{m=1}^{\infty}\sum_{n=0}^{\infty} r^{\lambda_m+n}\hat{W}_n^{(m)}(\theta,z)\right]e^{i\omega t}, \tag{7c}$$

$$\phi^*(r,\theta,z,t)=\left[\sum_{m=1}^{\infty}\sum_{n=0}^{\infty} r^{\lambda_m+n}\hat{\Phi}_n^{(m)}(\theta,z)\right]e^{i\omega t}, \tag{7d}$$

$$\psi^*(r,\theta,z,t)=\left[\sum_{m=1}^{\infty}\sum_{n=0}^{\infty} r^{\lambda_m+n}\hat{\Psi}_n^{(m)}(\theta,z)\right]e^{i\omega t}, \tag{7e}$$

The characteristic values λ_m may be real or complex for MEE wedges. For FGMEE wedges, λ_m is expected to depend on z because the material properties are functions of z. To ensure the finite displacements, electric field and magnetic field at $r=0$, the real part of λ_m (Re[λ_m]) is less than unity, the order of the singularities of stress, electric displacement and magnetic flux is Re[λ_m]-1.

Substituting Eqs. (7a)–(7e) into Eqs. (6a)–(6e), carefully rearranging and considering the terms with the lowest order of r yields,

$$\begin{aligned}&\frac{\partial^2\hat{U}_0^{(m)}}{\partial\theta^2}+p_1\frac{\partial\hat{U}_0^{(m)}}{\partial\theta}+p_2\hat{U}_0^{(m)}+p_3\frac{\partial^2\hat{V}_0^{(m)}}{\partial\theta^2}+p_4\frac{\partial\hat{V}_0^{(m)}}{\partial\theta}\\&+p_5\hat{V}_0^{(m)}+p_6\frac{\partial^2\hat{W}_0^{(m)}}{\partial\theta^2}+p_7\frac{\partial\hat{W}_0^{(m)}}{\partial\theta}+p_8\hat{W}_0^{(m)}\\&+p_9\frac{\partial^2\hat{\Phi}_0^{(m)}}{\partial\theta^2}+p_{10}\frac{\partial\hat{\Phi}_0^{(m)}}{\partial\theta}+p_{11}\hat{\Phi}_0^{(m)}+p_{12}\frac{\partial^2\hat{\Psi}_0^{(m)}}{\partial\theta^2}\\&+p_{13}\frac{\partial\hat{\Psi}_0^{(m)}}{\partial\theta}+p_{14}\hat{\Psi}_0^{(m)}=0,\end{aligned} \tag{8a}$$

$$\begin{aligned}&\frac{\partial^2\hat{V}_0^{(m)}}{\partial\theta^2}+q_1\frac{\partial\hat{V}_0^{(m)}}{\partial\theta}+q_2\hat{V}_0^{(m)}+q_3\frac{\partial^2\hat{U}_0^{(m)}}{\partial\theta^2}+q_4\frac{\partial\hat{U}_0^{(m)}}{\partial\theta}\\&+q_5\hat{U}_0^{(m)}+q_6\frac{\partial^2\hat{W}_0^{(m)}}{\partial\theta^2}+q_7\frac{\partial\hat{W}_0^{(m)}}{\partial\theta}+q_8\hat{W}_0^{(m)}\\&+q_9\frac{\partial^2\hat{\Phi}_0^{(m)}}{\partial\theta^2}+q_{10}\frac{\partial\hat{\Phi}_0^{(m)}}{\partial\theta}+q_{11}\hat{\Phi}_0^{(m)}+q_{12}\frac{\partial^2\hat{\Psi}_0^{(m)}}{\partial\theta^2}\\&+q_{13}\frac{\partial\hat{\Psi}_0^{(m)}}{\partial\theta}+q_{14}\hat{\Psi}_0^{(m)}=0,\end{aligned} \tag{8b}$$

$$\begin{aligned}&\frac{\partial^2\hat{W}_0^{(m)}}{\partial\theta^2}+r_1\frac{\partial\hat{W}_0^{(m)}}{\partial\theta}+r_2\hat{W}_0^{(m)}+r_3\frac{\partial^2\hat{U}_0^{(m)}}{\partial\theta^2}+r_4\frac{\partial\hat{U}_0^{(m)}}{\partial\theta}\\&+r_5\hat{U}_0^{(m)}+r_6\frac{\partial^2\hat{V}_0^{(m)}}{\partial\theta^2}+r_7\frac{\partial\hat{V}_0^{(m)}}{\partial\theta}+r_8\hat{V}_0^{(m)}\\&+r_9\frac{\partial^2\hat{\Phi}_0^{(m)}}{\partial\theta^2}+r_{10}\frac{\partial\hat{\Phi}_0^{(m)}}{\partial\theta}+r_{11}\hat{\Phi}_0^{(m)}+r_{12}\frac{\partial^2\hat{\Psi}_0^{(m)}}{\partial\theta^2}\\&+r_{13}\frac{\partial\hat{\Psi}_0^{(m)}}{\partial\theta}+r_{14}\hat{\Psi}_0^{(m)}=0,\end{aligned} \tag{8c}$$

$$\begin{aligned}&\frac{\partial^2\hat{\Phi}_0^{(m)}}{\partial\theta^2}+s_1\frac{\partial\hat{\Phi}_0^{(m)}}{\partial\theta}+s_2\hat{\Phi}_0^{(m)}+s_3\frac{\partial^2\hat{U}_0^{(m)}}{\partial\theta^2}+s_4\frac{\partial\hat{U}_0^{(m)}}{\partial\theta}\\&+s_5\hat{U}_0^{(m)}+s_6\frac{\partial^2\hat{V}_0^{(m)}}{\partial\theta^2}+s_7\frac{\partial\hat{V}_0^{(m)}}{\partial\theta}+s_8\hat{V}_0^{(m)}\\&+s_9\frac{\partial^2\hat{W}_0^{(m)}}{\partial\theta^2}+s_{10}\frac{\partial\hat{W}_0^{(m)}}{\partial\theta}+s_{11}\hat{W}_0^{(m)}+s_{12}\frac{\partial^2\hat{\Psi}_0^{(m)}}{\partial\theta^2}\\&+s_{13}\frac{\partial\hat{\Psi}_0^{(m)}}{\partial\theta}+s_{14}\hat{\Psi}_0^{(m)}=0,\end{aligned} \tag{8d}$$

$$\begin{aligned}&\frac{\partial^2\hat{\Psi}_0^{(m)}}{\partial\theta^2}+t_1\frac{\partial\hat{\Psi}_0^{(m)}}{\partial\theta}+t_2\hat{\Psi}_0^{(m)}+t_3\frac{\partial^2\hat{U}_0^{(m)}}{\partial\theta^2}+t_4\frac{\partial\hat{U}_0^{(m)}}{\partial\theta}+t_5\hat{U}_0^{(m)}\\&+t_6\frac{\partial^2\hat{V}_0^{(m)}}{\partial\theta^2}+t_7\frac{\partial\hat{V}_0^{(m)}}{\partial\theta}+t_8\hat{V}_0^{(m)}+t_9\frac{\partial^2\hat{W}_0^{(m)}}{\partial\theta^2}+t_{10}\frac{\partial\hat{W}_0^{(m)}}{\partial\theta}\\&+t_{11}\hat{W}_0^{(m)}+t_{12}\frac{\partial^2\hat{\Phi}_0^{(m)}}{\partial\theta^2}+t_{13}\frac{\partial\hat{\Phi}_0^{(m)}}{\partial\theta}+t_{14}\hat{\Phi}_0^{(m)}=0,\end{aligned} \tag{8e}$$

where p_i, q_i, r_i, s_i and t_i (i=1–14) are functions of θ and z and are defined in Appendix B. Careful examination of Eqs. (8a)–(8e) reveals that when λ_m at $z=z_l$ is sought, the material properties at $z=z_l$ must be used to determine p_i, q_i, r_i, s_i and t_i.

Eq. (8) represent a set of ordinary differential equations with variable coefficients. The three displacement components, electric potential and magnetic potential are generally coupled in Eqs. (8a)–(8e). The exact closed-form solutions to Eqs. (8a)–(8e) are intractable, if they exist. The power series method can be directly applied to establish a general solution to these ordinary differential equations. Very high-order terms are commonly needed to obtain an accurate solution and they typically cause numerical difficulties. To overcome these difficulties, a domain decomposition technique is applied in conjunction with the power series method to find a general solution to Eqs. (8a)–(8e).

The whole domain of θ is divided into numerous sub-domains (Fig. 2). A series solution for each sub-domain is constructed directly using the traditional power series method. Then, a general solution over the whole θ domain is obtained by assembling the solutions in all sub-domains and imposing continuity conditions between each pair of adjacent sub-domains. Notably, this solution procedure is also valid for a wedge that has different materials in different sub-domains of θ.

To develop the series solution for sub-domain i where $\theta_{i-1}\le\theta\le\theta_i$, the variable coefficients at $z=z_l$ in Eqs. (8a)–(8e) are expressed by Taylor's series with respect to the middle point of the sub-domain $\overline{\theta}_i$,

$$p_j(\theta,z_l)=\sum_{k=0}^{K}(\chi_j)_k^{(i)}(\theta-\overline{\theta}_i)^k,\quad q_j(\theta,z_l)=\sum_{k=0}^{K}(\kappa_j)_k^{(i)}(\theta-\overline{\theta}_i)^k,$$

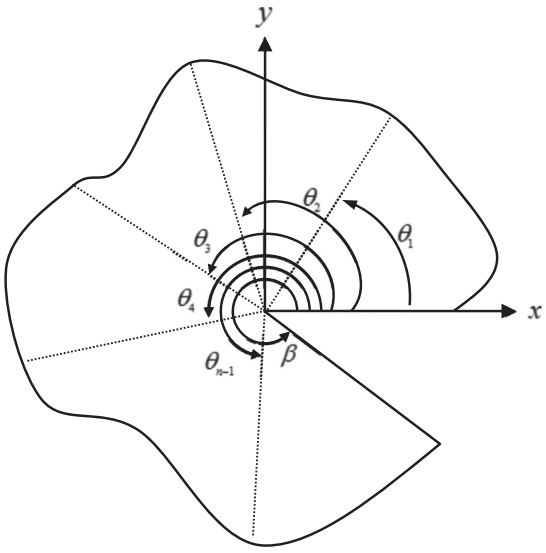

Fig. 2. Sub-domains for $\theta\in[0,\beta]$

$$r_j(\theta,z_l)=\sum_{k=0}^{K}(\vartheta_j)_k^{(i)}(\theta-\overline{\theta}_i)^k,\quad s_j(\theta,z_l)=\sum_{k=0}^{K}(\xi_j)_k^{(i)}(\theta-\overline{\theta}_i)^k,$$
$$t_j(\theta,z_l)=\sum_{k=0}^{K}(\zeta_j)_k^{(i)}(\theta-\overline{\theta}_i)^k. \tag{9}$$

Similarly, the solutions to Eqs. (8a)–(8e) in the sub-domain are expressed as

$$\hat{U}_{0i}^{(m)}=\sum_{j=0}^{J}\hat{A}_j^{(i)}(\theta-\overline{\theta}_i)^j,\quad \hat{V}_{0i}^{(m)}=\sum_{j=0}^{J}\hat{B}_j^{(i)}(\theta-\overline{\theta}_i)^j,$$
$$\hat{W}_{0i}^{(m)}=\sum_{j=0}^{J}\hat{C}_j^{(i)}(\theta-\overline{\theta}_i)^j,\quad \hat{\Phi}_{0i}^{(m)}=\sum_{j=0}^{J}\hat{D}_j^{(i)}(\theta-\overline{\theta}_i)^j$$
$$\hat{\Psi}_{0i}^{(m)}=\sum_{j=0}^{J}\hat{E}_j^{(i)}(\theta-\overline{\theta}_i)^j. \tag{10}$$

Substituting Eqs. (9) and (10) into Eqs. (8a)–(8e) yields the following recurrence relations among the coefficients in Eq. (10):

$$\begin{aligned}&\hat{A}_{j+2}^{(i)}+(\chi_3)_0^{(i)}\hat{B}_{j+2}^{(i)}+(\chi_6)_0^{(i)}\hat{C}_{j+2}^{(i)}+(\chi_9)_0^{(i)}\hat{D}_{j+2}^{(i)}+(\chi_{12})_0^{(i)}\hat{E}_{j+2}^{(i)}\\&=\frac{-1}{(j+2)(j+1)}\Bigg\{\sum_{k=0}^{j-1}\Bigg[(k+2)(k+1)\Big((\chi_3)_{j-k}^{(i)}\hat{B}_{k+2}^{(i)}+(\chi_6)_{j-k}^{(i)}\hat{C}_{k+2}^{(i)}\\&+(\chi_9)_{j-k}^{(i)}\hat{D}_{k+2}^{(i)}+(\chi_{12})_{j-k}^{(i)}\hat{E}_{k+2}^{(i)}\Big)\Bigg]\\&+\sum_{k=0}^{j}\Bigg[(k+1)\Big((\chi_1)_{j-k}^{(i)}\hat{A}_{k+1}^{(i)}+(\chi_4)_{j-k}^{(i)}\\&\times\hat{B}_{k+1}^{(i)}+(\chi_7)_{j-k}^{(i)}\hat{C}_{k+1}^{(i)}+(\chi_{10})_{j-k}^{(i)}\hat{D}_{k+1}^{(i)}+(\chi_{13})_{j-k}^{(i)}\hat{E}_{k+1}^{(i)}\Big)\\&+\Big((\chi_2)_{j-k}^{(i)}\hat{A}_k^{(i)}+(\chi_5)_{j-k}^{(i)}\hat{B}_k^{(i)}+(\chi_8)_{j-k}^{(i)}\hat{C}_k^{(i)}\\&+(\chi_{11})_{j-k}^{(i)}\hat{D}_k^{(i)}+(\chi_{14})_{j-k}^{(i)}\hat{E}_k^{(i)}\Big)\Bigg]\Bigg\},\end{aligned} \tag{11a}$$

$$\begin{aligned}&\hat{B}_{j+2}^{(i)}+(\kappa_3)_0^{(i)}\hat{A}_{j+2}^{(i)}+(\kappa_6)_0^{(i)}\hat{C}_{j+2}^{(i)}+(\kappa_9)_0^{(i)}\hat{D}_{j+2}^{(i)}+(\kappa_{12})_0^{(i)}\hat{E}_{j+2}^{(i)}\\&=\frac{-1}{(j+2)(j+1)}\Bigg\{\sum_{k=0}^{j-1}\Bigg[(k+2)(k+1)\times\Big((\kappa_3)_{j-k}^{(i)}\hat{A}_{k+2}^{(i)}+(\kappa_6)_{j-k}^{(i)}\hat{C}_{k+2}^{(i)}\\&+(\kappa_9)_{j-k}^{(i)}\hat{D}_{k+2}^{(i)}+(\kappa_{12})_{j-k}^{(i)}\hat{E}_{k+2}^{(i)}\Big)\Bigg]+\sum_{k=0}^{j}\Bigg[(k+1)\Big((\kappa_1)_{j-k}^{(i)}\hat{B}_{k+1}^{(i)}\\&+(\kappa_4)_{j-k}^{(i)}\times\hat{A}_{k+1}^{(i)}+(\kappa_7)_{j-k}^{(i)}\hat{C}_{k+1}^{(i)}+(\kappa_{10})_{j-k}^{(i)}\hat{D}_{k+1}^{(i)}+(\kappa_{13})_{j-k}^{(i)}\hat{E}_{k+1}^{(i)}\Big)\\&+\Big((\kappa_2)_{j-k}^{(i)}\hat{B}_k^{(i)}+(\kappa_5)_{j-k}^{(i)}\hat{A}_k^{(i)}+(\kappa_8)_{j-k}^{(i)}\hat{C}_k^{(i)}+(\kappa_{11})_{j-k}^{(i)}\hat{D}_k^{(i)}+(\kappa_{14})_{j-k}^{(i)}\hat{E}_k^{(i)}\Big)\Bigg]\Bigg\},\end{aligned} \tag{11b}$$

$$\begin{aligned}&\hat{C}_{j+2}^{(i)}+(\vartheta_3)_0^{(i)}\hat{A}_{j+2}^{(i)}+(\vartheta_6)_0^{(i)}\hat{B}_{j+2}^{(i)}+(\vartheta_9)_0^{(i)}\hat{D}_{j+2}^{(i)}+(\vartheta_{12})_0^{(i)}\hat{E}_{j+2}^{(i)}\\&=\frac{-1}{(j+2)(j+1)}\Bigg\{\sum_{k=0}^{j-1}\Bigg[(k+2)(k+1)\\&\times\Big((\vartheta_3)_{j-k}^{(i)}\hat{A}_{k+2}^{(i)}+(\vartheta_6)_{j-k}^{(i)}\hat{B}_{k+2}^{(i)}+(\vartheta_9)_{j-k}^{(i)}\hat{D}_{k+2}^{(i)}+(\vartheta_{12})_{j-k}^{(i)}\hat{E}_{k+2}^{(i)}\Big)\Bigg]\\&+\sum_{k=0}^{j}\Bigg[(k+1)\Big((\vartheta_1)_{j-k}^{(i)}\hat{C}_{k+1}^{(i)}+(\vartheta_4)_{j-k}^{(i)}\\&\times\hat{A}_{k+1}^{(i)}+(\vartheta_7)_{j-k}^{(i)}\hat{B}_{k+1}^{(i)}+(\vartheta_{10})_{j-k}^{(i)}\hat{D}_{k+1}^{(i)}+(\vartheta_{13})_{j-k}^{(i)}\hat{E}_{k+1}^{(i)}\Big)\\&+\Big((\vartheta_2)_{j-k}^{(i)}\hat{C}_k^{(i)}+(\vartheta_5)_{j-k}^{(i)}\hat{A}_k^{(i)}+(\vartheta_8)_{j-k}^{(i)}\hat{B}_k^{(i)}\\&+(\vartheta_{11})_{j-k}^{(i)}\hat{D}_k^{(i)}+(\vartheta_{14})_{j-k}^{(i)}\hat{E}_k^{(i)}\Big)\Bigg]\Bigg\},\end{aligned} \tag{11c}$$

$$\begin{aligned}&\hat{D}_{j+2}^{(i)}+(\xi_3)_0^{(i)}\hat{A}_{j+2}^{(i)}+(\xi_6)_0^{(i)}\hat{B}_{j+2}^{(i)}+(\xi_9)_0^{(i)}\hat{C}_{j+2}^{(i)}+(\xi_{12})_0^{(i)}\hat{E}_{j+2}^{(i)}\\&=\frac{-1}{(j+2)(j+1)}\Bigg\{\sum_{k=0}^{j-1}\Bigg[(k+2)(k+1)\\&\times\Big((\xi_3)_{j-k}^{(i)}\hat{A}_{k+2}^{(i)}+(\xi_6)_{j-k}^{(i)}\hat{B}_{k+2}^{(i)}+(\xi_9)_{j-k}^{(i)}\hat{C}_{k+2}^{(i)}+(\xi_{12})_{j-k}^{(i)}\hat{E}_{k+2}^{(i)}\Big)\Bigg]\\&+\sum_{k=0}^{j}\Bigg[(k+1)\Big((\xi_1)_{j-k}^{(i)}\hat{D}_{k+1}^{(i)}+(\xi_4)_{j-k}^{(i)}\cdot\\&\times\hat{A}_{k+1}^{(i)}+(\xi_7)_{j-k}^{(i)}\hat{B}_{k+1}^{(i)}+(\xi_{10})_{j-k}^{(i)}\hat{C}_{k+1}^{(i)}+(\xi_{13})_{j-k}^{(i)}\hat{E}_{k+1}^{(i)}\Big)\\&+\Big((\xi_2)_{j-k}^{(i)}\hat{D}_k^{(i)}+(\xi_5)_{j-k}^{(i)}\hat{A}_k^{(i)}+(\xi_8)_{j-k}^{(i)}\hat{B}_k^{(i)}\\&+(\xi_{11})_{j-k}^{(i)}\hat{C}_k^{(i)}+(\xi_{14})_{j-k}^{(i)}\hat{E}_k^{(i)}\Big)\Bigg]\Bigg\},\end{aligned} \tag{11d}$$

$$\begin{aligned}&\hat{E}_{j+2}^{(i)}+(\xi_3)_0^{(i)}\hat{A}_{j+2}^{(i)}+(\xi_6)_0^{(i)}\hat{B}_{j+2}^{(i)}+(\xi_9)_0^{(i)}\hat{C}_{j+2}^{(i)}+(\xi_{12})_0^{(i)}\hat{D}_{j+2}^{(i)}\\&=\frac{-1}{(j+2)(j+1)}\Bigg\{\sum_{k=0}^{j-1}\Bigg[(k+2)(k+1)\\&\times\Big((\xi_3)_{j-k}^{(i)}\hat{A}_{k+2}^{(i)}+(\xi_6)_{j-k}^{(i)}\hat{B}_{k+2}^{(i)}+(\xi_9)_{j-k}^{(i)}\hat{C}_{k+2}^{(i)}+(\xi_{12})_{j-k}^{(i)}\hat{D}_{k+2}^{(i)}\Big)\Bigg]\\&+\sum_{k=0}^{j}\Bigg[(k+1)\Big((\xi_1)_{j-k}^{(i)}\hat{E}_{k+1}^{(i)}+(\xi_4)_{j-k}^{(i)}\\&\times\hat{A}_{k+1}^{(i)}+(\xi_7)_{j-k}^{(i)}\hat{B}_{k+1}^{(i)}+(\xi_{10})_{j-k}^{(i)}\hat{C}_{k+1}^{(i)}+(\xi_{13})_{j-k}^{(i)}\hat{D}_{k+1}^{(i)}\Big)\\&+\Big((\xi_2)_{j-k}^{(i)}\hat{E}_k^{(i)}+(\xi_5)_{j-k}^{(i)}\hat{A}_k^{(i)}+(\xi_8)_{j-k}^{(i)}\hat{B}_k^{(i)}\\&+(\xi_{11})_{j-k}^{(i)}\hat{C}_k^{(i)}+(\xi_{14})_{j-k}^{(i)}\hat{D}_k^{(i)}\Big)\Bigg]\Bigg\},\end{aligned} \tag{11e}$$

Careful examination of Eqs. (11a)–(11e) reveals that the coefficients $\hat{A}_j^{(i)}$, $\hat{B}_j^{(i)}$, $\hat{C}_j^{(i)}$, $\hat{D}_j^{(i)}$ and $\hat{E}_j^{(i)}$ with $j\geq 2$ are determined from Eqs. (11a)–(11e) if $\hat{A}_0^{(i)}$, $\hat{A}_1^{(i)}$, $\hat{B}_0^{(i)}$, $\hat{B}_1^{(i)}$, $\hat{C}_0^{(i)}$, $\hat{C}_1^{(i)}$, $\hat{D}_0^{(i)}$, $\hat{D}_1^{(i)}$, $\hat{E}_0^{(i)}$ and $\hat{E}_1^{(i)}$ are known. As a result, the solutions of Eqs. (8a)–(8e) in sub-domain i can be expressed as

$$\begin{aligned}\hat{U}_{0i}^{(m)}(\theta,z)=&\hat{A}_0^{(i)}\hat{U}_{0i0}^{(m)}(\theta,z)+\hat{A}_1^{(i)}\hat{U}_{0i1}^{(m)}(\theta,z)+\hat{B}_0^{(i)}\hat{U}_{0i2}^{(m)}(\theta,z)\\&+\hat{B}_1^{(i)}\hat{U}_{0i3}^{(m)}(\theta,z)+\hat{C}_0^{(i)}\hat{U}_{0i4}^{(m)}(\theta,z)\\&+\hat{C}_1^{(i)}\hat{U}_{0i5}^{(m)}(\theta,z)+\hat{D}_0^{(i)}\hat{U}_{0i6}^{(m)}(\theta,z)+\hat{D}_1^{(i)}\hat{U}_{0i7}^{(m)}(\theta,z)\\&+\hat{E}_0^{(i)}\hat{U}_{0i8}^{(m)}(\theta,z)+\hat{E}_1^{(i)}\hat{U}_{0i9}^{(m)}(\theta,z),\end{aligned} \tag{12a}$$

$$\begin{aligned}\hat{V}_{0i}^{(m)}(\theta,z)=&\hat{A}_0^{(i)}\hat{V}_{0i0}^{(m)}(\theta,z)+\hat{A}_1^{(i)}\hat{V}_{0i1}^{(m)}(\theta,z)+\hat{B}_0^{(i)}\hat{V}_{0i2}^{(m)}(\theta,z)\\&+\hat{B}_1^{(i)}\hat{V}_{0i3}^{(m)}(\theta,z)+\hat{C}_0^{(i)}\hat{V}_{0i4}^{(m)}(\theta,z)\\&+\hat{C}_1^{(i)}\hat{V}_{0i5}^{(m)}(\theta,z)+\hat{D}_0^{(i)}\hat{V}_{0i6}^{(m)}(\theta,z)+\hat{D}_1^{(i)}\hat{V}_{0i7}^{(m)}(\theta,z)\\&+\hat{E}_0^{(i)}\hat{V}_{0i8}^{(m)}(\theta,z)+\hat{E}_1^{(i)}\hat{V}_{0i9}^{(m)}(\theta,z),\end{aligned} \tag{12b}$$

$$\begin{aligned}\hat{W}_{0i}^{(m)}(\theta,z)=&\hat{A}_0^{(i)}\hat{W}_{0i0}^{(m)}(\theta,z)+\hat{A}_1^{(i)}\hat{W}_{0i1}^{(m)}(\theta,z)+\hat{B}_0^{(i)}\hat{W}_{0i2}^{(m)}(\theta,z)\\&+\hat{B}_1^{(i)}\hat{W}_{0i3}^{(m)}(\theta,z)+\hat{C}_0^{(i)}\hat{W}_{0i4}^{(m)}(\theta,z)+\hat{C}_1^{(i)}\hat{W}_{0i5}^{(m)}(\theta,z)\\&+\hat{D}_0^{(i)}\hat{W}_{0i6}^{(m)}(\theta,z)+\hat{D}_1^{(i)}\hat{W}_{0i7}^{(m)}(\theta,z)+\hat{E}_0^{(i)}\hat{W}_{0i8}^{(m)}(\theta,z)\\&+\hat{E}_1^{(i)}\hat{W}_{0i9}^{(m)}(\theta,z),\end{aligned} \tag{12c}$$

$$\begin{aligned}\hat{\Phi}_{0i}^{(m)}(\theta,z)=&\hat{A}_0^{(i)}\hat{\Phi}_{0i0}^{(m)}(\theta,z)+\hat{A}_1^{(i)}\hat{\Phi}_{0i1}^{(m)}(\theta,z)+\hat{B}_0^{(i)}\hat{\Phi}_{0i2}^{(m)}(\theta,z)\\&+\hat{B}_1^{(i)}\hat{\Phi}_{0i3}^{(m)}(\theta,z)+\hat{C}_0^{(i)}\hat{\Phi}_{0i4}^{(m)}(\theta,z)\\&+\hat{C}_1^{(i)}\hat{\Phi}_{0i5}^{(m)}(\theta,z)+\hat{D}_0^{(i)}\hat{\Phi}_{0i6}^{(m)}(\theta,z)+\hat{D}_1^{(i)}\hat{\Phi}_{0i7}^{(m)}(\theta,z)\\&+\hat{E}_0^{(i)}\hat{\Phi}_{0i9}^{(m)}(\theta,z)+\hat{E}_1^{(i)}\hat{\Phi}_{0i9}^{(m)}(\theta,z),\end{aligned} \tag{12d}$$

$$\hat{\Psi}_{0i}^{(m)}(\theta,z)=\hat{A}_0^{(i)}\hat{\Psi}_{0i0}^{(m)}(\theta,z)+\hat{A}_1^{(i)}\hat{\Psi}_{0i1}^{(m)}(\theta,z)+\hat{B}_0^{(i)}\hat{\Psi}_{0i2}^{(m)}(\theta,z)+\hat{B}_1^{(i)}\hat{\Psi}_{0i3}^{(m)}(\theta,z)+\hat{C}_0^{(i)}\hat{\Psi}_{0i4}^{(m)}(\theta,z)+\hat{C}_1^{(i)}\hat{\Psi}_{0i5}^{(m)}(\theta,z)+\hat{D}_0^{(i)}\hat{\Psi}_{0i6}^{(m)}(\theta,z)+\hat{D}_1^{(i)}\hat{\Psi}_{0i7}^{(m)}(\theta,z)+\hat{E}_0^{(i)}\hat{\Psi}_{0i9}^{(m)}(\theta,z)+\hat{E}_1^{(i)}\hat{\Psi}_{0i9}^{(m)}(\theta,z), \quad (12e)$$

Dividing the overall domain of θ into n sub-domains yields $10n$ coefficients $\hat{A}_0^{(i)}$, $\hat{A}_1^{(i)}$, $\hat{B}_0^{(i)}$, $\hat{B}_1^{(i)}$, $\hat{C}_0^{(i)}$, $\hat{C}_1^{(i)}$, $\hat{D}_0^{(i)}$, $\hat{D}_1^{(i)}$, $\hat{E}_0^{(i)}$ and $\hat{E}_1^{(i)}$ for $i=1, 2, \ldots n$, which are to be determined. The continuity conditions between pairs of adjacent sub-domains provide $10(n-1)$ equations, which are, at $\theta=\theta_i$ ($i=1, 2, \ldots, n\text{-}1$)

$$u_{r(i)}^*=u_{r(i+1)}^*,\quad u_{\theta(i)}^*=u_{\theta(i+1)}^*,\quad u_{z(i)}^*=u_{z(i+1)}^*, \quad (13a)$$

$$\sigma_{r\theta(i)}^*=\sigma_{r\theta(i+1)}^*,\quad \sigma_{\theta\theta(i)}^*=\sigma_{\theta\theta(i+1)}^*,\quad \sigma_{z\theta(i)}^*=\sigma_{z\theta(i+1)}^*, \quad (13b)$$

$$D_{\theta(i)}^*=D_{\theta(i+1)}^*,\quad \phi_{(i)}^*=\phi_{(i+1)}^*,\quad B_{\theta(i)}^*=B_{\theta(i+1)}^*,\quad \psi_{(i)}^*=\psi_{(i+1)}^*. \quad (13c)$$

The homogenous boundary conditions at $\theta=0$ and $\theta=\beta$ give another 10 equations. The homogeneous boundary conditions can be specified as follows:

$$\sigma_{r\theta}^*=\sigma_{\theta\theta}^*=\sigma_{z\theta}^*=0 \text{ (tractionfree) or } u_r^*=u_\theta^*=u_z^*=0 \text{ (clamped)}, \quad (14a)$$

$$D_\theta^*=B_\theta^*=0 \text{ (magneto}-\text{electrically open)} \quad \text{or}$$
$$\phi^*=\psi^*=0 \text{ (magneto}-\text{electrically closed)}, \quad (14b)$$

Table 1
Material properties.

Parameters	$BaTiO_3$ [37]	$CoFe_2O_4$ [37]
$\bar{c}_{11}$ (GPa)	166	286.0
$\bar{c}_{12}$ (GPa)	77	173.0
$\bar{c}_{13}$ (GPa)	78	170.5
$\bar{c}_{33}$ (GPa)	162	269.5
$\bar{c}_{44}$ (GPa)	43	45.3
$\bar{e}_{15}$ (C/m^2)	11.6	0
$\bar{e}_{31}$ (C/m^2)	−4.4	0
$\bar{e}_{33}$ (C/m^2)	18.6	0
$\bar{d}_{15}$ (N/Am)	0	550.0
$\bar{d}_{31}$ (N/Am)	0	580.3
$\bar{d}_{33}$ (N/Am)	0	699.7
$\bar{\eta}_{11}$ (C^2/Nm^2)	112.0×10^{-10}	0.8×10^{-10}
$\bar{\eta}_{33}$ (C^2/Nm^2)	126.0×10^{-10}	0.93×10^{-10}
$\bar{\mu}_{11}$ (Ns^2/C^2)	5.0×10^{-6}	590.0×10^{-6}
$\bar{\mu}_{33}$ (Ns^2/C^2)	10.0×10^{-6}	157.0×10^{-6}
$\bar{g}_{11}$(Ns/VC)	0	0
$\bar{g}_{33}$(Ns/VC)	0	0

Consequently, $10n$ homogeneous algebraic equations are established for the $10n$ coefficients to be determined. To have nontrivial solutions for the coefficients requires zero determinant of the $10n\times10n$ matrix that is formed from the coefficients in the established $10n$ homogeneous algebraic equations. The values of λ_m are the roots of the zero determinant and are determined by the numerical approach of Müller [35]; they are ordered as $\mathrm{Re}[\lambda_i] \le \mathrm{Re}[\lambda_{i+1}]$ ($i=1, 2, 3,\ldots$).

4. Verification and comparison

The $BaTiO_3$–$CoFe_2O_4$ particulate composite is a typical MEE material and is considered herein. According to the macroscopic mixture rule, the composite material properties of this MEE material are related to the material properties of $BaTiO_3$ and $CoFe_2O_4$ by [36]

$$\bar{\kappa}_{ij}=\bar{\kappa}_{ij}^B V_I+\bar{\kappa}_{ij}^F(1-V_I), \quad (15)$$

where $\bar{\kappa}_{ij}^B$ and $\bar{\kappa}_{ij}^F$ denote the material properties of $BaTiO_3$ and $CoFe_2O_4$ (Table 1), respectively, and V_I is the volume fraction of the

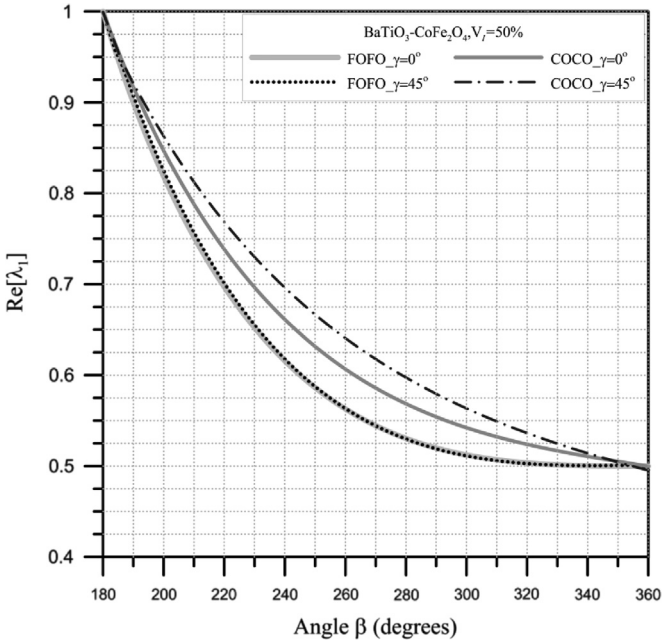

Fig. 3. Variation of $\mathrm{Re}[\lambda_1]$ with vertex angle for MEE wedges.

Table 2
Convergence of $\mathrm{Re}[\lambda_1]$ for MEE wedges.

Vertex angle	Material	Boundary conditions	Number of sub-domains	Terms								Published results
				6	7	8	9	10	12	14	15	
$\beta=360^\circ$	$BaTiO_3$–$CoFe_2O_4V_I=50\%$	FOCO	3	0.2482	0.2492	0.2462	0.2489	0.2492	0.2495	0.2499	0.2499	0.2500 [32]
			4	0.2504	0.2501	0.2500	0.2498	0.2495	0.2500	0.2500	0.2500	
			6	0.2500	0.2499	0.2500	0.2500	0.2500	0.2500	0.2500	0.2500	
			8	0.2500	0.2500	0.2500	0.2500	0.2500	0.2500	0.2500	0.2500	
	$BaTiO_3$–$CoFe_2O_4V_I^{(1)}/V_I^{(2)}=50\%/20\%$	FOFO	3	0.4978	0.4916	0.4417	0.4980	0.4998	0.4750	0.5000	0.4999	0.5000 [32]
			4	0.4963	0.4993	0.4999	0.4999	0.4984	0.4999	0.4999	0.4999	
			6	0.4993	0.4999	0.4999	0.5000	0.5000	0.4999	0.5000	0.5000	
			8	0.4999	0.4999	0.4999	0.4999	0.5000	0.5000	0.4999	0.5000	
	$BaTiO_3$–$CoFe_2O_4V_I^{(1)}/V_I^{(2)}=90\%/10\%$		3	0.4962	0.4933	0.4823	0.4887	0.4978	0.4983	0.4999	0.4999	0.5000 [32]
			4	0.4977	0.4972	0.4986	0.4998	0.4989	0.4998	0.4999	0.4999	
			6	0.4993	0.4996	0.4999	0.5000	0.5000	0.4999	0.5000	0.5000	
			8	0.4999	0.5000	0.4998	0.5000	0.5000	0.5000	0.5000	0.5000	

inclusion $BaTiO_3$. The material properties in Table 1 were taken from Wang et al. [37].

For simplicity, four letters are utilized to specify the boundary conditions along the two radial side faces of a wedge with vertex angle β. The first and third letters indicate mechanical boundary conditions at $\theta=0$ and $\theta=\beta$, respectively; C and F specify clamped and traction-free, respectively. Similarly, the second and fourth letters represent the magneto-electric boundary conditions at $\theta=0$ and $\theta=\beta$, respectively; C and O denote magneto-electrically closed and open boundary conditions, respectively.

Since MEE singularities in an MEE wedge that is subjected to the out-of-plane deformation and in-plane electric and magnetic fields have been studied, wedges with the direction of polarization along the z axis are analyzed herein to verify the proposed solutions. For such wedges, the out-of-plane deformation and in-plane electric and magnetic fields are independent of in-plane deformation and out-of-plane electric and magnetic fields according to Eqs. (6a)–(6e). Notably, Eqs. (8a)–(8e) are independent of z for an MEE wedge. Consequently, the results of Liu and Chue [32], who assumed that all physical quantities are independent of z, are used for comparison.

Table 2 shows values of $\mathrm{Re}[\lambda_1]$ that were obtained by the present approach and by that of Liu and Chue [32] for three wedges with a vertex angle $\beta=360^\circ$. One wedge is made of $BaTiO_3$ and $CoFe_2O_4$ with $V_I=50\%$ under FOCO boundary conditions. The other two are under FOFO boundary conditions and made of $BaTiO_3$ and $CoFe_2O_4$ with $V_I=50\%$ and 90% for $0^\circ\le\theta<180^\circ$ and with $V_I=20\%$ and 10% for

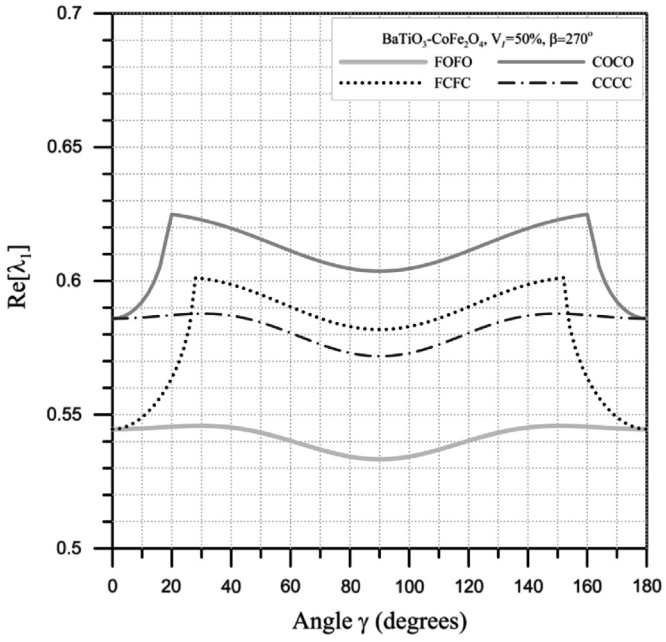

Fig. 4. Variation of $\mathrm{Re}[\lambda_1]$ with polarization direction for MEE wedges with $\beta=270^\circ$.

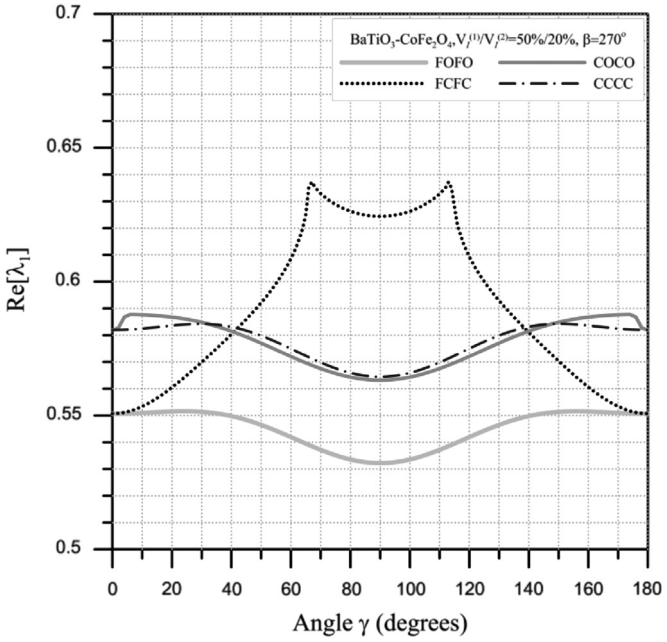

Fig. 6. Variation of $\mathrm{Re}[\lambda_1]$ with polarization direction for bi-material MEE wedges with $\beta=270^\circ$.

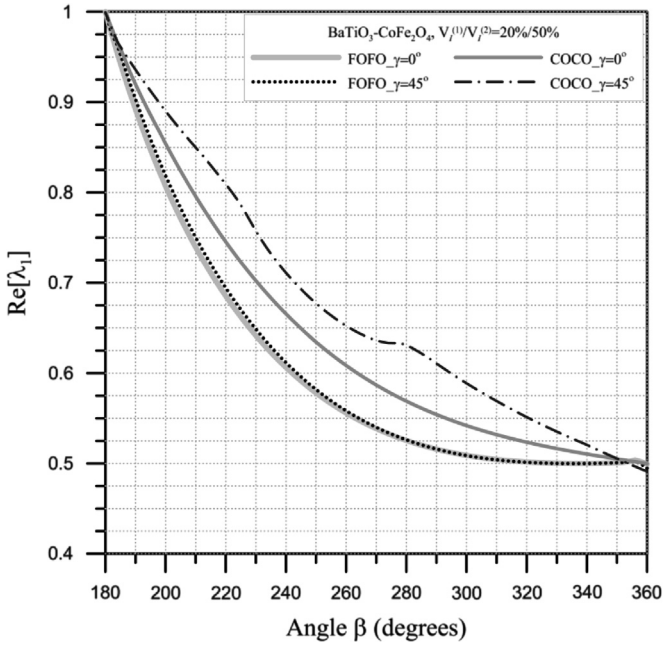

Fig. 5. Variation of $\mathrm{Re}[\lambda_1]$ with vertex angle for bi-material MEE wedges.

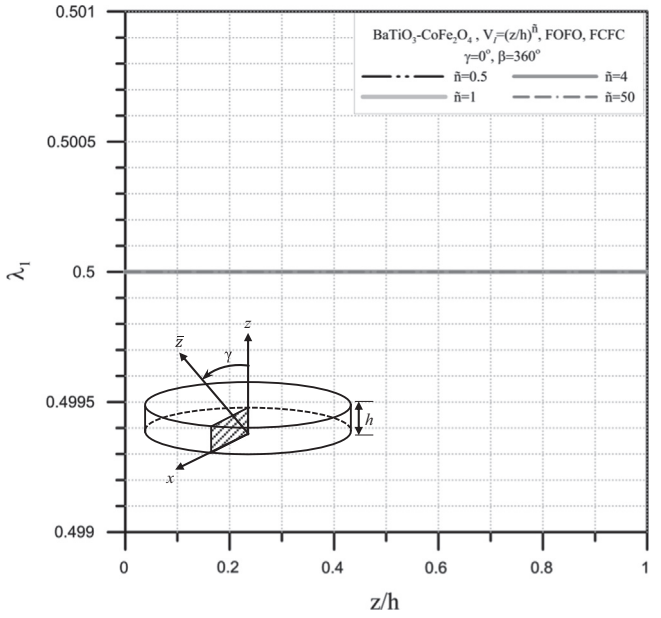

Fig. 7. Distribution of λ_1 along the thicknesses of FGMEE wedges with $\gamma=0^\circ$ and $\beta=360^\circ$.

$180^\circ < \theta \leq 360^\circ$, respectively. Notably, for comparison, $\bar{\mu}_{11} = 100 \times 10^{-6}$ Ns^2/C^2 for $CoFe_2O_4$, as in the work of Liu and Chue [32] was used for the results in Table 2. The present results were obtained using different numbers of sub-domains and polynomial terms for each sub-domain. The convergent results were obtained by increasing the number of sub-domains or the number of polynomial terms for each sub-domain. The convergent results agree excellently with the results of Liu and Chue [32].

5. Numerical results and discussion

Following the confirmation of the correctness of the proposed solution, the asymptotic solution is further employed to investigate the MEE singularities in the MEE and FGMEE wedges, taking into account the effects of the polarization direction, vertex angle, material-property gradient index and boundary conditions. In the following, only Re[λ_1] is shown in a graphic form because the dominant singularity order at the vertex of a wedge depends on Re[λ_1]. Notably, the vertical axis of a figure is labeled λ_1 when all λ_1 are real; otherwise, the vertical axis is labeled Re[λ_1]. The numerical results were obtained by dividing a wedge into eight sub-domains in θ with 10 polynomial terms per sub-domain. The $\bar{x}$–$\bar{y}$–$\bar{z}$ coordinate system is formed by rotating the x–y–z coordinate system counter-clockwise about the y-axis through an angle γ, so the angle between the polarization direction of an MEE or FGMEE wedge and its thickness direction is γ.

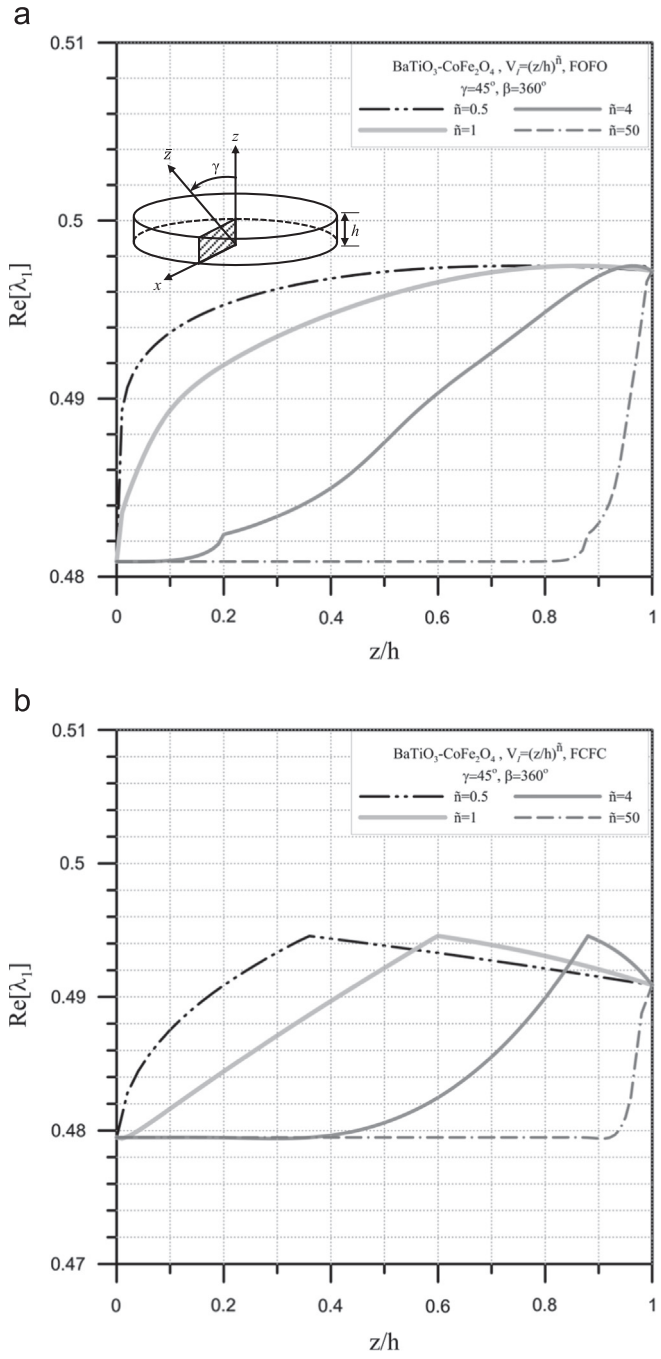

Fig. 8. Distribution of Re[λ_1] along the thicknesses of FGMEE wedges with $\gamma = 45^\circ$ and $\beta = 360^\circ$: (a) FOFO boundary conditions, and (b) FCFC boundary conditions.

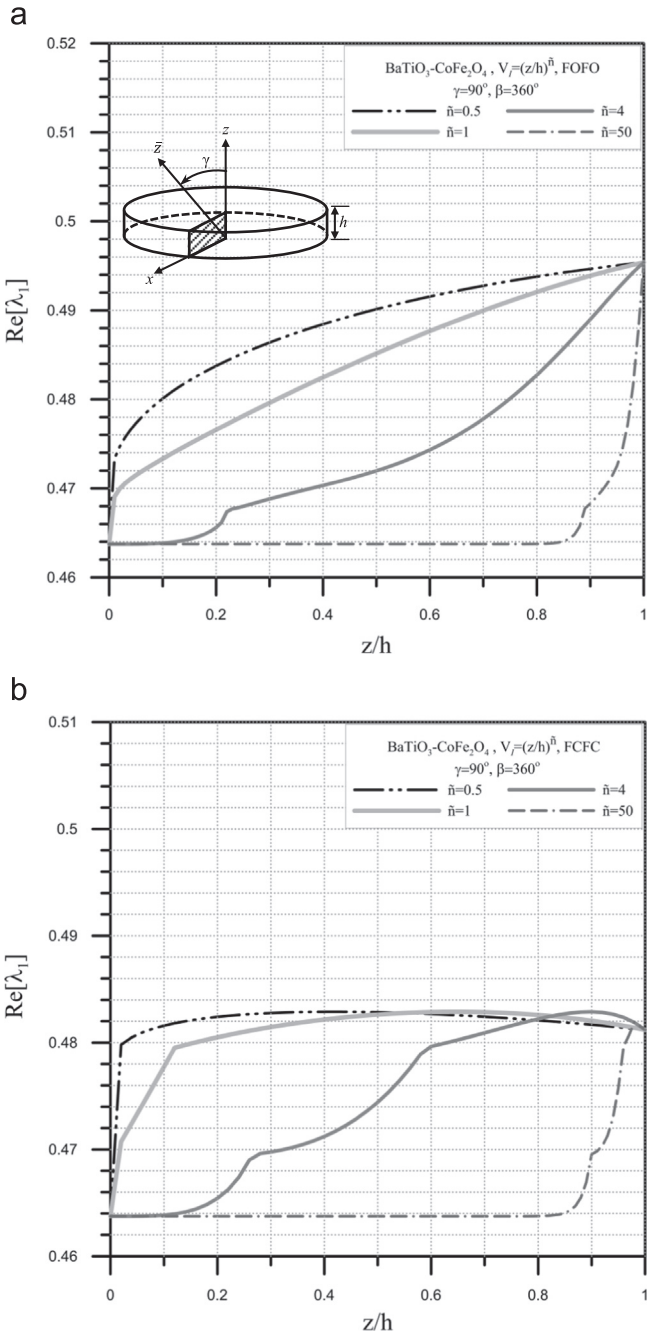

Fig. 9. Distribution of Re[λ_1] along the thicknesses of FGMEE wedges with $\gamma = 90^\circ$ and $\beta = 360^\circ$: (a) FOFO boundary conditions, and (b) FCFC boundary conditions.

5.1. MEE wedges

Figs. 3 and 4 show the results concerning Re[λ_1] for $BaTiO_3$–$CoFe_2O_4$ wedges with $V_I = 50\%$ and different polarization directions and boundary conditions. Fig. 3 plots the variation of Re[λ_1] with the vertex angle β, whereas Fig. 4 depicts the variation of Re[λ_1] with the polarization direction for wedges with $\beta = 270^\circ$. Notably, some values of λ_1 in Figs. 3 and 4 are complex. For example, all λ_1 values in Fig. 3 for wedges with $\gamma = 45^\circ$ and COCO boundary conditions are complex, and λ_1 values in Fig. 4 for wedges with γ between 28° and 152° under FCFC boundary conditions are complex. These figures demonstrate that the strength of MEE singularities in a wedge generally increases with β, and that free–free mechanical boundary conditions lead to stronger singularities than clamped–clamped boundary conditions. Fig. 4 indicates that changing the direction of polarization can change Re[λ_1] by up to approximately 10%.

The arrangements considered in Figs. 5 and 6 are the same as those in Figs. 3 and 4, respectively, except that bi-material wedges are considered in Figs. 5 and 6. The bi-material wedges in Fig. 5 are made of $BaTiO_3$–$CoFe_2O_4$ with $V_I = 50\%$ in $0^\circ \le \theta < 180^\circ$ and $BaTiO_3$–$CoFe_2O_4$ with $V_I = 20\%$ in $180^\circ < \theta \le \beta$. Fig. 5 also reveals that Re[λ_1] generally decreases as β increases. Notably, not all values of λ_1 are complex for wedges with COCO boundary conditions and $\gamma = 45^\circ$, and λ_1 is real when β is between 212° and 336°. Fig. 6 considers bi-material wedges with β=270°, made of $BaTiO_3$-$CoFe_2O_4$ with V_I=20% in $0^\circ \le \theta < 180^\circ$ and $BaTiO_3$-$CoFe_2O_4$ with V_I=50% in $180^\circ < \theta \le 270^\circ$, and indicates that indicates that changing the polarization direction can change Re[λ_1] by up to around 15%.

5.2. FGMEE wedges

As mentioned in Section 1, no investigation of geometrically-induced singularities in an FGMEE wedge has been published. The special feature of the graded spatial compositions of FGMEE materials enables these materials to be used in a very wide range of applications. The distribution of the singularities at the vertex of an FGMEE wedge along its thickness is of particular interest.

FGMEE wedges under consideration herein consist of $BaTiO_3$–$CoFe_2O_4$ with V_I varying along the thickness direction according to a simple power law

$$V_I = \left(\frac{z}{h}\right)^{\tilde{n}}, \tag{16}$$

where $\tilde{n}$ is the material-property gradient index, which indicates the degree of variation of the material properties along its thickness h, and $0 \le z \le h$. The wedges consist of $CoFe_2O_4$ only at their bottom surfaces ($z=0$), and $BaTiO_3$ at their top surfaces ($z=h$).

Figs. 7, 8, and 9 display the variations of Re[λ_1] or λ_1 along the thickness of the FGMEE wedges with γ=0°, 45° and 90°, respectively. The wedges have vertex angle $\beta = 360^\circ$, free–free mechanical

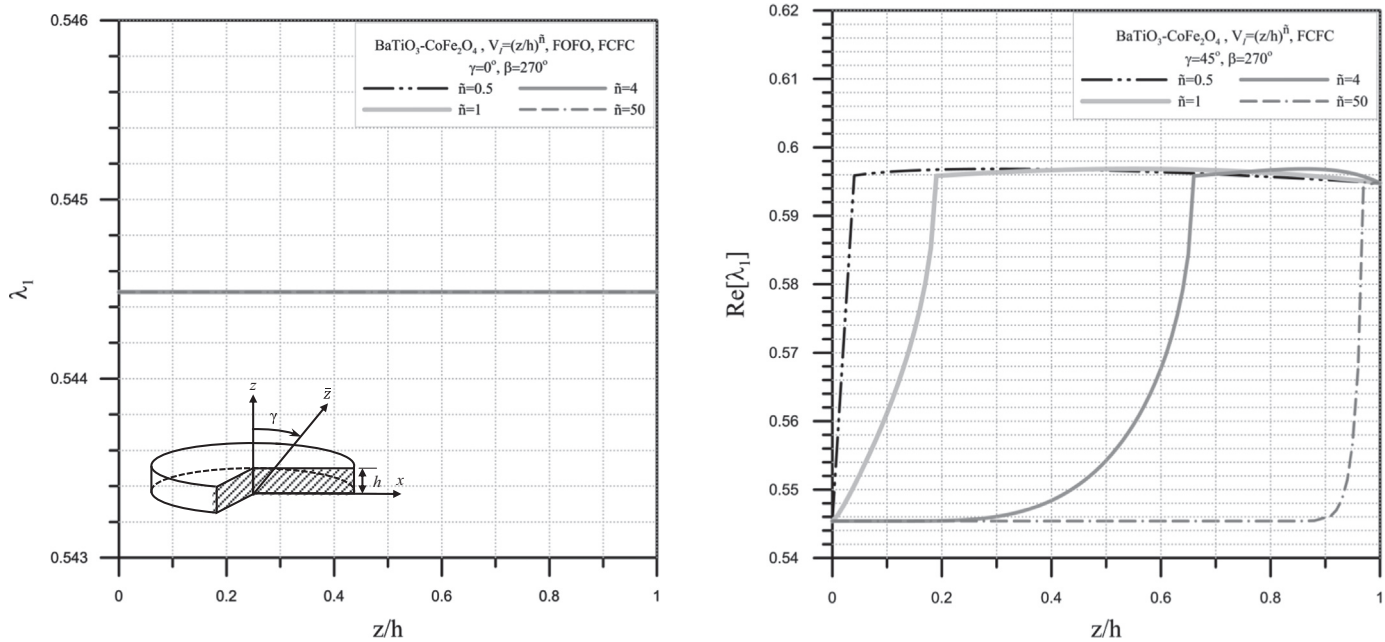

Fig. 10. Distribution of λ_1 along the thicknesses of FGMEE wedges with $\gamma = 0^\circ$ and $\beta = 270^\circ$.

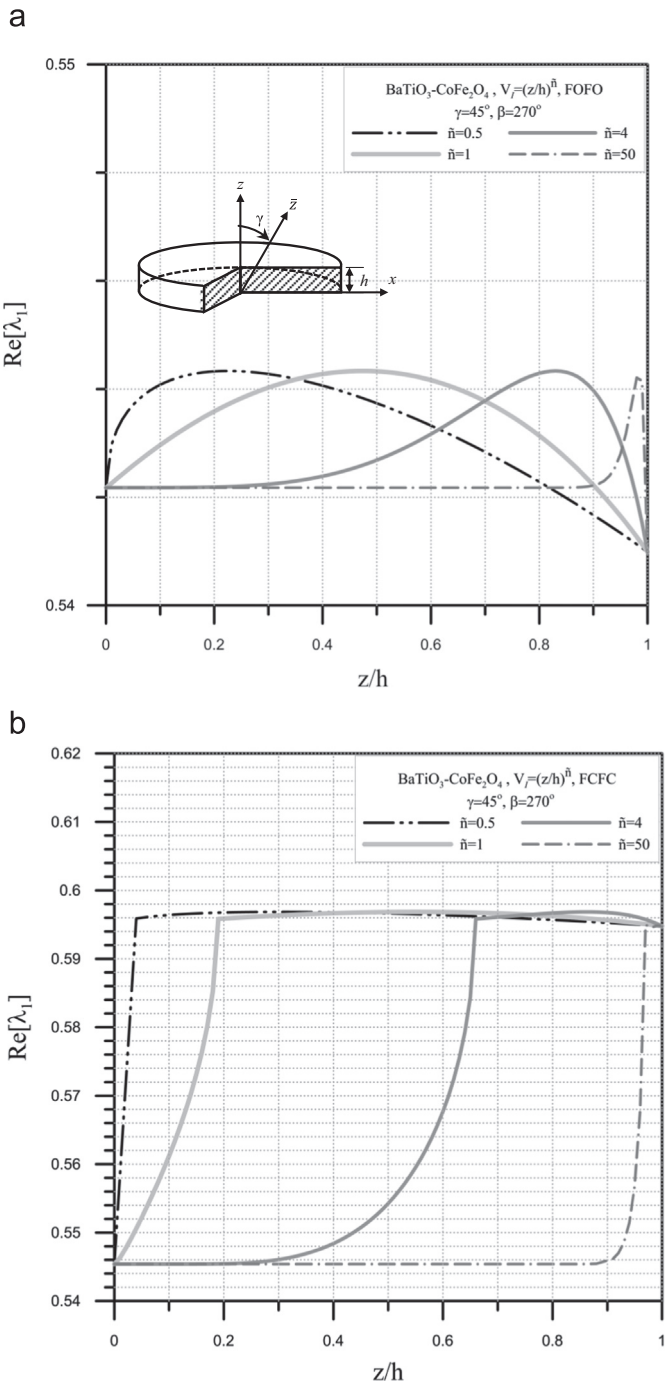

Fig. 11. Distribution of Re[λ_1] along the thicknesses of FGMEE wedges with $\gamma = 45^\circ$ and $\beta = 270^\circ$: (a) FOFO boundary conditions, and (b) FCFC boundary conditions.

boundary conditions and $\tilde{n}=0.5$, 1, 4 and 50. Fig. 7 demonstrates that for wedges with $\gamma=0^\circ$ under FOFO and FCFC boundary conditions, the material-property gradient index does not affect the strength of the singularities at the vertex ($\lambda_1=0.5$), which remains constant along the thickness direction. Boundary conditions FOFO and FCFC yield identical results. Figs. 8 and 9 reveal that when $\gamma=45^\circ$ and 90°, the values of $\mathrm{Re}[\lambda_1]$ vary with z/h and $\tilde{n}$ by less than 7%. The values of $\mathrm{Re}[\lambda_1]$ for wedges with FOFO boundary conditions generally increase with an increase of z/h and a decrease in $\tilde{n}$, but these trends are not observed under FCFC boundary conditions.

The arrangements considered in Figs. 10, 11 and 12 are the same as those in Figs. 7, 8, and 9, respectively, except that wedges with $\beta=270^\circ$ are considered in Figs. 10–12. Fig. 10 reveals that $\mathrm{Re}[\lambda_1]$ does not depend on z/h or $\tilde{n}$ for wedges with $\gamma=0^\circ$ under FOFO or FCFC boundary conditions, and boundary conditions FOFO and FCFC yield identical results. Figs. 11 and 12 discover that $\mathrm{Re}[\lambda_1]$ may significantly depend on z/h and $\tilde{n}$, and $\mathrm{Re}[\lambda_1]$ may vary by about 4% and 12% for FOFO and FCFC wedges, respectively. The values of $\mathrm{Re}[\lambda_1]$ for wedges

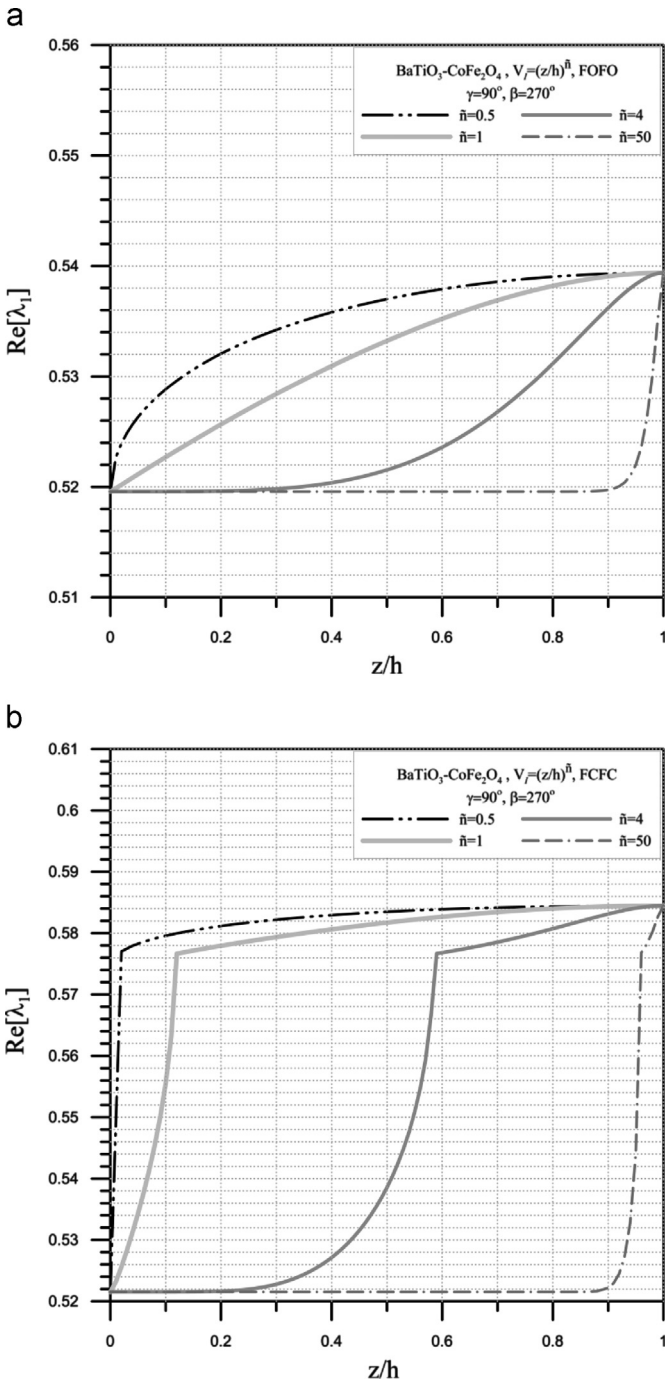

Fig. 12. Distribution of $\mathrm{Re}[\lambda_1]$ along the thicknesses of FGMEE wedges with $\gamma=90^\circ$ and $\beta=270^\circ$: (a) FOFO boundary conditions, and (b) FCFC boundary conditions.

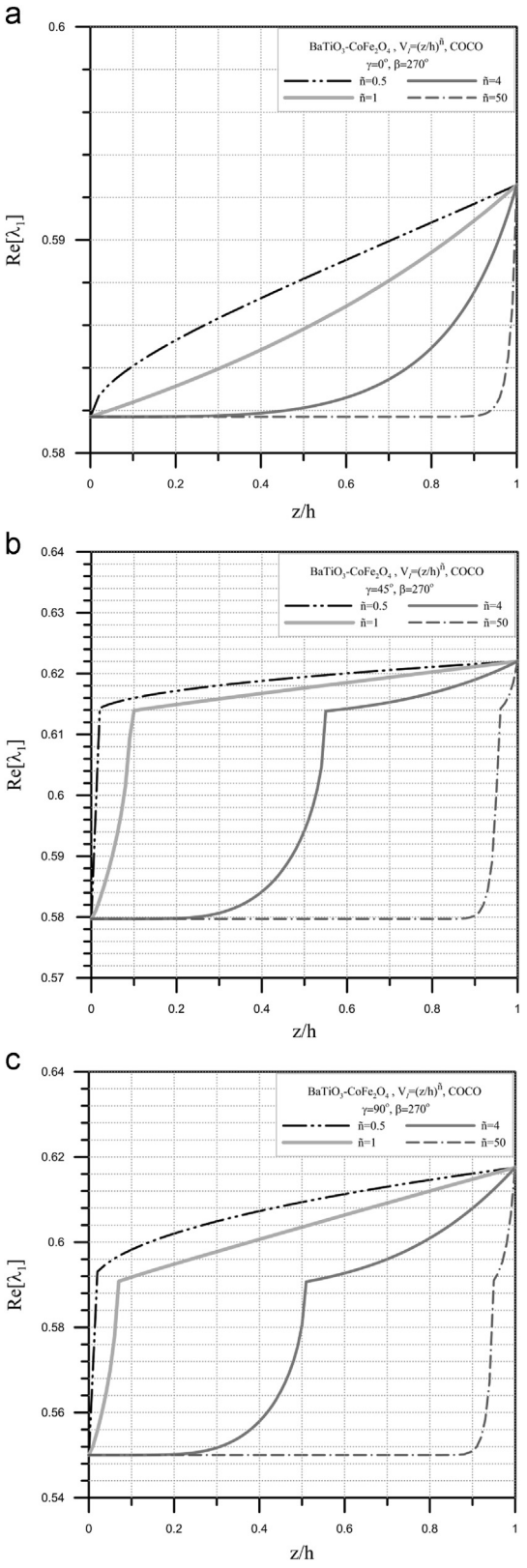

Fig. 13. Distribution of $\mathrm{Re}[\lambda_1]$ with along the thicknesses of FGMEE wedges with $\beta=270^\circ$ and COCO boundary conditions: (a) $\gamma=0^\circ$, (b) $\gamma=45^\circ$, and (c) $\gamma=90^\circ$.

with $\gamma = 90^\circ$ generally increase with increasing z/h and decreasing $\tilde{n}$, but wedges with $\gamma = 45^\circ$ do not exhibit these trends.

To investigate the effects of mechanical boundary conditions on Re[λ_1], Fig. 13 depicts the variation of Re[λ_1] or λ_1 along the thickness direction of COCO wedges with $\beta = 270^\circ$ and various γ ($\gamma = 0^\circ$, 45° and 90°) and $\tilde{n}$($\tilde{n} = 0.5$, 1, 4 and 50). The values of Re[λ_1] generally increase with an increase in z/h or a decrease in $\tilde{n}$. The variations of λ_1 with z/h and $\tilde{n}$ are less than 2% for wedges with $\gamma = 0^\circ$, and Re[λ_1] may vary by up to 7% and 13% for $\gamma = 45^\circ$ and 90°, respectively.

6. Concluding remarks

Based on three-dimensional magneto-electro-elasticity theory, this study established asymptotic solutions for the geometrically-induced magneto-electro-elastic singularities at the vertex of a rectilinearly polarized wedge that is made of functionally graded magneto-electro-elastic materials. The asymptotic solutions were developed using an eigenfunction expansion approach with the power series solution technique and a domain decomposition technique to solve the three-dimensional equations of motion and Maxwell's equations in terms of mechanical displacement components and electric and magnetic potentials in a cylindrical coordinate system. An arbitrary polarization direction of material yields coupling among in-plane and out-of-plane physical quantities (mechanical displacement, electric and magnetic fields), considerably complicates the asymptotic solutions. The correctness of the solutions was confirmed by performing convergence studies of Re[λ_1] for $BaTiO_3$–$CoFe_2O_4$ wedges with polarization in the thickness direction, and comparing the convergent Re[λ_1] with the results published for wedges under anti-plane deformation and in-plane electric and magnetic fields.

The proposed solutions were further employed to determine the variations of Re[λ_1] with the vertex angle (β) and the position along the thickness (z/h) for MEE and FGMEE wedges made of $BaTiO_3$–$CoFe_2O_4$ particulate composite under various boundary conditions and with various polarization directions ($\gamma = 0^\circ$, 45° and 90°). For FGMEE wedges, the volume fraction of the inclusion $BaTiO_3$ was assumed to vary in the thickness direction in a manner governed by a simple power law with the material-property gradient index, and the effects of the material-property gradient index ($\tilde{n} = 0.5$, 1, 4, and 50) on Re[λ_1] were examined.

Numerical results reveal that a larger vertex angle yields stronger MEE singularities at the vertex of a wedge, and free–free mechanical boundary conditions lead to stronger singularities than do clamped–clamped boundary conditions. The polarization direction may significantly affect Re[λ_1]. When FGMEE wedges are polarized along the thickness direction ($\gamma = 0^\circ$), $\tilde{n}$ and z/h have no effect on the orders of singularities in the wedges with $\beta = 270^\circ$ and 360° under FOFO or FCFC boundary conditions. When the thickness direction is not the direction of polarization, the orders of singularities in an FGMEE wedge may depend significantly on $\tilde{n}$ and z/h. For example, Re[λ_1] may vary with $\tilde{n}$ and z/h by up to about 12% for a wedge with $\beta = 270^\circ$, $\gamma = 90^\circ$ under FCFC boundary conditions. Notably, the variation of orders of singularities with z/h substantially complicates the determination of stress intensity factors for an FGMEE plate with a V-notch or crack.

Acknowledgment

The authors would like to thank the National Science Council of the Republic of China, Taiwan, for financially supporting this research under Contract no. NSC 102-2221-E-009-071.

Appendix A

$[c] = [\mathbf{T}]_\sigma[\mathbf{K}][\overline{c}][\mathbf{K}]^T[\mathbf{T}]_\varepsilon^{-1}$, $[e] = [\mathbf{T}]_D[\mathbf{L}][\overline{e}][\mathbf{K}]^T[\mathbf{T}]_\varepsilon^{-1}$, $[d] = [\mathbf{T}]_D[\mathbf{L}]\left[\overline{d}\right][\mathbf{K}]^T[\mathbf{T}]_\varepsilon^{-1}$,
$[\eta] = [\mathbf{T}]_D[\mathbf{L}][\overline{\eta}][\mathbf{L}]^T[\mathbf{T}]_E^{-1}$, $[\mu] = [\mathbf{T}]_B[\mathbf{L}][\overline{\mu}][\mathbf{L}]^T[\mathbf{T}]_H^{-1}$, $[g] = [\mathbf{T}]_E[\mathbf{L}][\overline{g}][\mathbf{L}]^T[\mathbf{T}]_B^{-1}$

where

$$[\mathbf{T}]_\sigma = \begin{bmatrix} \cos^2\theta & \sin^2\theta & 0 & 2\cos\theta\sin\theta & 0 & 0 \\ \sin^2\theta & \cos^2\theta & 0 & -2\cos\theta\sin\theta & 0 & 0 \\ 0 & 0 & 1 & 0 & 0 & 0 \\ -\cos\theta\sin\theta & \cos\theta\sin\theta & 0 & \cos^2\theta-\sin^2\theta & 0 & 0 \\ 0 & 0 & 0 & 0 & \cos\theta & \sin\theta \\ 0 & 0 & 0 & 0 & -\sin\theta & \cos\theta \end{bmatrix},$$

$$[\mathbf{T}]_\varepsilon = \begin{bmatrix} \cos^2\theta & \sin^2\theta & 0 & \cos\theta\sin\theta & 0 & 0 \\ \sin^2\theta & \cos^2\theta & 0 & -\cos\theta\sin\theta & 0 & 0 \\ 0 & 0 & 1 & 0 & 0 & 0 \\ -2\cos\theta\sin\theta & 2\cos\theta\sin\theta & 0 & \cos^2\theta-\sin^2\theta & 0 & 0 \\ 0 & 0 & 0 & 0 & \cos\theta & \sin\theta \\ 0 & 0 & 0 & 0 & -\sin\theta & \cos\theta \end{bmatrix},$$

$$[\mathbf{T}]_E = [\mathbf{T}]_D = [\mathbf{T}]_B = [\mathbf{T}]_H = \begin{bmatrix} \cos\theta & \sin\theta & 0 \\ -\sin\theta & \cos\theta & 0 \\ 0 & 0 & 1 \end{bmatrix},$$

$$[\mathbf{L}] = \begin{bmatrix} \cos(x,\overline{x}) & \cos(x,\overline{y}) & \cos(x,\overline{z}) \\ \cos(y,\overline{x}) & \cos(y,\overline{y}) & \cos(y,\overline{z}) \\ \cos(z,\overline{x}) & \cos(z,\overline{y}) & \cos(z,\overline{z}) \end{bmatrix} = \begin{bmatrix} l_{11} & l_{12} & l_{13} \\ l_{21} & l_{22} & l_{23} \\ l_{31} & l_{32} & l_{33} \end{bmatrix},$$

$$[\mathbf{K}] = \begin{bmatrix} \mathbf{K}_1 & 2\mathbf{K}_2 \\ \mathbf{K}_3 & \mathbf{K}_4 \end{bmatrix}, \quad \mathbf{K}_1 = \begin{bmatrix} l_{11}^2 & l_{12}^2 & l_{13}^2 \\ l_{21}^2 & l_{22}^2 & l_{23}^2 \\ l_{31}^2 & l_{32}^2 & l_{33}^2 \end{bmatrix},$$

$$\mathbf{K}_2 = \begin{bmatrix} l_{12}l_{13} & l_{13}l_{11} & l_{11}l_{12} \\ l_{22}l_{23} & l_{23}l_{21} & l_{21}l_{22} \\ l_{32}l_{33} & l_{33}l_{31} & l_{31}l_{32} \end{bmatrix},$$

$$\mathbf{K}_3 = \begin{bmatrix} l_{21}l_{31} & l_{22}l_{32} & l_{23}l_{33} \\ l_{31}l_{11} & l_{32}l_{12} & l_{33}l_{13} \\ l_{11}l_{21} & l_{12}l_{22} & l_{13}l_{23} \end{bmatrix},$$

$$\mathbf{K}_4 = \begin{bmatrix} l_{22}l_{33}+l_{23}l_{32} & l_{23}l_{31}+l_{21}l_{33} & l_{21}l_{32}+l_{22}l_{31} \\ l_{32}l_{13}+l_{33}l_{12} & l_{33}l_{11}+l_{31}l_{13} & l_{31}l_{12}+l_{32}l_{11} \\ l_{12}l_{23}+l_{13}l_{22} & l_{13}l_{21}+l_{11}l_{23} & l_{11}l_{22}+l_{12}l_{21} \end{bmatrix}.$$

Appendix B

$$p_1 = \frac{1}{c_{66}}\left(2\lambda_m c_{16} + \frac{\partial c_{66}}{\partial\theta}\right), \quad p_2 = \frac{1}{c_{66}}\left(\lambda_m^2 c_{11} + \lambda_m\frac{\partial c_{16}}{\partial\theta} - c_{22} + \frac{\partial c_{26}}{\partial\theta}\right),$$

$$p_3 = \frac{c_{26}}{c_{66}}, \quad p_4 = \frac{1}{c_{66}}\left[(\lambda_m - 1)c_{66} + \lambda_m c_{12} - c_{22} + \frac{\partial c_{26}}{\partial\theta}\right],$$

$$p_5 = \frac{1}{c_{66}}(\lambda_m - 1)\left(\lambda_m c_{16} - c_{26} + \frac{\partial c_{66}}{\partial\theta}\right), \quad p_6 = \frac{c_{46}}{c_{66}},$$

$$p_7 = \frac{1}{c_{66}}\left[\lambda_m(c_{14} + c_{56}) - c_{24} + \frac{\partial c_{46}}{\partial\theta}\right],$$

$$p_8 = \frac{1}{c_{66}}\lambda_m\left(\lambda_m c_{15} - c_{25} + \frac{\partial c_{56}}{\partial\theta}\right), \quad p_9 = \frac{e_{26}}{c_{66}},$$

$$p_{10} = \frac{1}{c_{66}}\left[\lambda_m(e_{16} + e_{21}) - e_{22} + \frac{\partial e_{26}}{\partial\theta}\right],$$

$$p_{11} = \frac{1}{c_{66}}\lambda_m\left(\lambda_m e_{11} - e_{12} + \frac{\partial e_{16}}{\partial\theta}\right), \quad p_{12} = \frac{d_{26}}{c_{66}},$$

$$p_{13} = \frac{1}{c_{66}}\left[\lambda_m(d_{16} + d_{21}) - d_{22} + \frac{\partial d_{26}}{\partial\theta}\right],$$

$$p_{14}=\frac{1}{c_{66}}\lambda_m\left(\lambda_m d_{11}-d_{12}+\frac{\partial d_{16}}{\partial\theta}\right).$$

$$q_1=\frac{1}{c_{22}}\left(2\lambda_m c_{26}+\frac{\partial c_{22}}{\partial\theta}\right),\quad q_2=\frac{1}{c_{22}}(\lambda_m-1)\left[(\lambda_m+1)c_{66}+\frac{\partial c_{26}}{\partial\theta}\right],$$
$$q_3=\frac{c_{26}}{c_{22}},\quad q_4=\frac{1}{c_{22}}\left[\lambda_m(c_{12}+c_{66})+c_{66}+c_{22}+\frac{\partial c_{26}}{\partial\theta}\right],$$
$$q_5=\frac{1}{c_{22}}\left[(\lambda_m+1)(\lambda_m c_{16}+c_{26})+\lambda_m\frac{\partial c_{12}}{\partial\theta}+\frac{\partial c_{22}}{\partial\theta}\right],$$
$$q_6=\frac{c_{24}}{c_{22}},\quad q_7=\frac{1}{c_{22}}\left[\lambda_m(c_{25}+c_{46})+c_{46}+\frac{\partial c_{24}}{\partial\theta}\right],$$
$$q_8=\lambda_m\left[(\lambda_m+1)c_{56}+\frac{\partial c_{25}}{\partial\theta}\right],$$
$$q_9=\frac{e_{22}}{c_{22}},\quad q_{10}=\frac{1}{c_{22}}\left[\lambda_m(e_{12}+e_{26})+e_{26}+\frac{\partial e_{22}}{\partial\theta}\right],$$
$$q_{11}=\frac{1}{c_{22}}\lambda_m\left[(\lambda_m+1)e_{16}+\frac{\partial e_{12}}{\partial\theta}\right],$$
$$q_{12}=\frac{d_{22}}{c_{22}},\quad q_{13}=\frac{1}{c_{22}}\left[\lambda_m(d_{12}+d_{26})+d_{26}+\frac{\partial d_{22}}{\partial\theta}\right],$$
$$q_{14}=\frac{1}{c_{22}}\lambda_m\left[(\lambda_m+1)d_{16}+\frac{\partial d_{12}}{\partial\theta}\right].$$

$$r_1=\frac{1}{c_{44}}\left(2\lambda_m c_{45}+\frac{\partial c_{44}}{\partial\theta}\right),\quad r_2=\frac{1}{c_{44}}\lambda_m\left(\lambda_m c_{55}+\frac{\partial c_{45}}{\partial\theta}\right),\quad r_3=\frac{c_{46}}{c_{44}}$$
$$r_4=\frac{1}{c_{44}}\left[\lambda_m(c_{14}+c_{56})+c_{24}+\frac{\partial c_{46}}{\partial\theta}\right],$$
$$r_5=\frac{1}{c_{44}}\left[\lambda_m\left(\lambda_m c_{15}+c_{25}+\frac{\partial c_{14}}{\partial\theta}\right)+\frac{\partial c_{24}}{\partial\theta}\right],\quad r_6=\frac{c_{24}}{c_{44}},$$
$$r_7=\frac{1}{c_{44}}\left[\lambda_m(c_{25}+c_{46})-c_{46}+\frac{\partial c_{24}}{\partial\theta}\right],$$
$$r_8=\frac{1}{c_{44}}(\lambda_m-1)\left(\lambda_m c_{56}+\frac{\partial c_{46}}{\partial\theta}\right),\quad r_9=\frac{e_{24}}{c_{44}},$$
$$r_{10}=\frac{1}{c_{44}}\left[\lambda_m(e_{14}+e_{25})+\frac{\partial e_{24}}{\partial\theta}\right],\quad r_{11}=\frac{1}{c_{44}}\lambda_m\left(\lambda_m e_{15}+\frac{\partial e_{14}}{\partial\theta}\right),$$
$$r_{12}=\frac{d_{24}}{c_{44}},r_{13}=\frac{1}{c_{44}}\left[\lambda_m(d_{14}+d_{25})+\frac{\partial d_{24}}{\partial\theta}\right],$$
$$r_{14}=\frac{1}{c_{44}}\lambda_m\left(\lambda_m d_{15}+\frac{\partial d_{14}}{\partial\theta}\right).$$

$$s_1=\frac{1}{\eta_{22}}\left(2\lambda_m\eta_{12}+\frac{\partial\eta_{22}}{\partial\theta}\right),\quad s_2=\frac{1}{\eta_{22}}\lambda_m\left(\lambda_m\eta_{11}+\frac{\partial\eta_{12}}{\partial\theta}\right),\quad s_3=-\frac{e_{26}}{\eta_{22}},$$
$$s_4=-\frac{1}{\eta_{22}}\left[\lambda_m(e_{16}+e_{21})+e_{22}+\frac{\partial e_{26}}{\partial\theta}\right],$$
$$s_5=-\frac{1}{\eta_{22}}\left[\lambda_m\left(\lambda_m e_{11}+e_{12}+\frac{\partial e_{21}}{\partial\theta}\right)+\frac{\partial e_{22}}{\partial\theta}\right]$$
$$s_6=-\frac{e_{22}}{\eta_{22}},\quad s_7=-\frac{1}{\eta_{22}}\left[\lambda_m(e_{12}+e_{26})-e_{26}+\frac{\partial e_{22}}{\partial\theta}\right],$$
$$s_8=-\frac{1}{\eta_{22}}(\lambda_m-1)\left(\lambda_m e_{16}+\frac{\partial e_{26}}{\partial\theta}\right),$$
$$s_9=-\frac{e_{24}}{\eta_{22}},\quad s_{10}=-\frac{1}{\eta_{22}}\left[\lambda_m(e_{14}+e_{25})+\frac{\partial e_{24}}{\partial\theta}\right],$$
$$s_{11}=-\frac{1}{\eta_{22}}\lambda_m\left(\lambda_m e_{15}+\frac{\partial e_{25}}{\partial\theta}\right),$$
$$s_{12}=\frac{g_{22}}{\eta_{22}},\quad s_{13}=\frac{1}{\eta_{22}}\left[2\lambda_m g_{12}+\frac{\partial g_{22}}{\partial\theta}\right],$$
$$s_{14}=\frac{1}{\eta_{22}}\lambda_m\left(\lambda_m g_{11}+\frac{\partial g_{12}}{\partial\theta}\right).$$

$$t_1=\frac{1}{\mu_{22}}\left(2\lambda_m\mu_{12}+\frac{\partial\mu_{22}}{\partial\theta}\right),\quad t_2=\frac{1}{\mu_{22}}\lambda_m\left(\lambda_m\mu_{11}+\frac{\partial\mu_{12}}{\partial\theta}\right),\quad t_3=-\frac{d_{26}}{\mu_{22}},$$
$$t_4=-\frac{1}{\mu_{22}}\left[\lambda_m(d_{16}+d_{21})+d_{22}+\frac{\partial d_{26}}{\partial\theta}\right],$$
$$t_5=-\frac{1}{\mu_{22}}\left[\lambda_m\left(\lambda_m d_{11}+d_{12}+\frac{\partial d_{21}}{\partial\theta}\right)+\frac{\partial d_{22}}{\partial\theta}\right],$$
$$t_6=-\frac{d_{22}}{\mu_{22}},\quad t_7=-\frac{1}{\mu_{22}}\left[\lambda_m(d_{12}+d_{26})-d_{26}+\frac{\partial d_{22}}{\partial\theta}\right],$$
$$t_8=-\frac{1}{\mu_{22}}(\lambda_m-1)\left(\lambda_m d_{16}+\frac{\partial d_{26}}{\partial\theta}\right),$$
$$t_9=-\frac{d_{24}}{\mu_{22}},\quad t_{10}=-\frac{1}{\mu_{22}}\left[\lambda_m(d_{14}+d_{25})+\frac{\partial d_{24}}{\partial\theta}\right],$$
$$t_{11}=-\frac{1}{\mu_{22}}\lambda_m\left(\lambda_m d_{15}+\frac{\partial d_{25}}{\partial\theta}\right),$$
$$t_{12}=\frac{g_{22}}{\mu_{22}},\quad t_{13}=\frac{1}{\mu_{22}}\left[2\lambda_m g_{12}+\frac{\partial g_{22}}{\partial\theta}\right],$$
$$t_{14}=\frac{1}{\mu_{22}}\lambda_m\left(\lambda_m g_{11}+\frac{\partial g_{12}}{\partial\theta}\right).$$

References

[1] Sinclair GB. Stress singularities in classical elasticity – I: removal, interpretation, and analysis. Appl Mech Rev 2004;57(4):251–97.
[2] Williams ML. Stress singularities resulting from various boundary conditions in angular corners of plates under bending. In: Proceeding of the 1st U.S. National Congress of applied mechanics; 1952. p. 325–9.
[3] Williams ML. Stress singularities resulting from various boundary conditions in angular corners of plates in extension. J Appl Mech 1952;19:526–8.
[4] Bogy DB, Wang KC. Stress singularities at interface corners in bonded dissimilar isotropic elastic materials. Int J Solids Struct 1971;7:993–1005.
[5] Dempsey JP, Sinclair GB. On the stress singularities in the plate elasticity of the composite wedge. J Elast 1979;9(4):373–91.
[6] Dempsey JP, Sinclair GB. On the stress singular behavior at the vertex of a bi-material wedge. J Elast 1981;11(3):317–27.
[7] Hein VL, Erdogan F. Stress singularities in a two-material wedge. Int J Fract Mech 1971;7:317–30.
[8] Rao AK. Stress concentrations and singularities at interfaces corners. Z Angew Math Mech 1971;51:395–406.
[9] Ting TCT, Chou SC. Edge singularities in anisotropic composites. Int J Solids Struct 1981;17(11):1057–68.
[10] Kuo MC, Bogy DB. Plane solutions for the displacement and traction-displacement problems for anisotropic elastic wedges. J Appl Mech 1974;41(1):197–202.
[11] Lin YY, Sung JC. Stress singularities at the apex of a dissimilar anisotropic wedge. ASME J Appl Mech 1998;65(2):454–63.
[12] Chen HP. Stress singularities in anisotropic multi-material wedges and junctions. Int J Solids Struct 1998;35(11):1057–73.
[13] Burton WS, Sinclair GB. On the singularities in Reissner's theory for the bending of elastic plates. J Appl Mech 1986;53(1):220–2.
[14] Huang CS. On the singularity induced by boundary conditions in a third-order thick plate theory. ASME J Appl Mech 2002;69(6):800–10.
[15] Huang CS. Stress singularities at angular corners in first-order shear deformation plate theory. Int J Mech Sci 2003;45(1):1–20.
[16] McGee OG, Kim JW. Sharp corners functions for Mindlin plates. ASME J Appl Mech 2005;72(1):1–9.
[17] Hartranft RJ, Sih GC. The use of eigenfunction expansions in the general solution of three-dimensional crack problems. J Math Mech 1969;19:123–38.
[18] Xie M, Chaudhuri RA. Three-dimensional stress singularity at a bimaterial interface crack front. Compos Struct 1997;40(2):137–47.
[19] Huang CS, Chang MJ. Corner stress singularities in a FGM thin plate. Int J Solids Struc 2007;44(9):2802–19.
[20] Huang CS, Chang MJ. Geometrically induced stress singularities of a thick FGM plate based on the third-order shear deformation theory. Mech Adv Mater Struct 2009;16(2):83–97.
[21] Xu XL, Rajapakse RKND. On singularities in composite piezoelectric wedges and junctions. Int J Solids Struc 2000;37(23):3235–75.
[22] Shang F, Kitamura T. On stress singularity at the interface edge between piezoelectric thin film and elastic substrate. Microsyst Technol 2005;11(8–10):1115–20.
[23] Wang Z, Zheng B. The general solution of three dimensional problems in piezoelectric media. Int J Solids Struct 1995;32(1):105–15.
[24] Hwu C, Ikeda T. Eletromechanical fracture analysis for corners and cracks in piezoelectric materials. Int J Solids Struct 2008;45(22–23):5744–64.
[25] Chue CH, Chen CD. Decoupled formulation of piezoelectric elasticity under generalized plane deformation and its application to wedge problems. Int J Solids Struct 2002;39(12):3131–58.
[26] Chue CH, Chen CD. Antiplane stress singularities in a bonded bimaterial piezoelectric wedge. Arch Appl Mech 2003;72(9):673–85.
[27] Chen TH, Chue CH, Lee HT. Stress singularities near the apex of a cylindrically polarized piezoelectric wedge. Arch Appl Mech 2004;74(3–4):248–61.
[28] Scherzer M, Kuna M. Combined analytical and numerical solution of 2D interface corner configurations between dissimilar piezoelectric materials. Int J Fract 2004;127(1):61–99.

[29] Chen MC, Zhu JJ, Sze KY. Electroelastic singularities in piezoelectric-elastic wedges and junctions. Eng Fract Mech 2006;73(7):855–68.
[30] Chen MC, Ping XC. Finite element analysis of piezoelectric corner configurations and cracks accounting for different electrical permeabilities. Eng Fract Mech 2007;74(9):1511–24.
[31] Huang CS, Hu CN. Three-dimensional analyses of stress singularities at the vertex of a piezoelectric wedge. Appl Math Model 2013;37(6):4517–37.
[32] Liu TJC, Chue CH. On the singularities in a bimaterial magneto-electro-elastic composite wedge under antiplane deformation. Compos Struct 2006;72(2):254–65.
[33] Sue WC, Liou JY, Sung JC. Investigation of the stress singularity of a magnetoelectroelastic bonded antiplane wedge. Appl Math Model 2007;31(10):2313–31.
[34] Liu TJC. The singularity problem of the magneto-electro-elastic wedge-junction structure with consideration of the air effect. Arch Appl Mech 2009;79(5):377–93.
[35] Müller DE. A method for solving algebraic equations using an automatic computer. Math Tables Other Aids Comput 1956;10:208–15.
[36] Song ZF, Sih GC. Crack initiation behavior in magnetoelectroelastic composite under in-plane deformation. Theor Appl Fract Mech 2003;39(3):189–207.
[37] Wang Y, Xu R, Ding H. Axisymmetric bending of functionally graded circular magneto-electro-elastic plates. Eur J Mech – A/Solids 2011;30(6):999–1011.